Temperature elevation synergises with and enhances the type-I IFN-mediated restriction of MPXV

Chris Davis[1], Ilaria Epifano[1], Kieran Dee[1], Steven McFarlane[1], Joanna K. Wojtus, Benjamin Brennan[1], Quan Gu[1], Sreenu B. Vattipally[1], Kyriaki Nomikou[1], Lily Tong[1], Lauren Orr[1], Ana Da Silva Filipe[1], Antonia Ho[1], Emma C. Thomson[1], Chris Boutell[1*].

[1] MRC-University of Glasgow Centre for Virus Research (CVR), Glasgow, Scotland (UK)

*chris.boutell@glasgow.ac.uk

Running title: Temperature elevation inhibits monkeypox virus replication

Abstract

Mpox (formerly monkeypox) is a zoonotic disease caused by the monkeypox virus (MPXV). In January 2022, the World Health Organization (WHO) reported a global outbreak in mpox cases across all six WHO regions with a high incidence rate of human-to-human transmission. A frequent prodrome symptom of MPXV infection is fever, with a febrile range of 38.3 to 40.5 °C. Fever is an evolutionary conserved host pro-inflammatory immune response to infection that can influence multiple biological processes. However, the outcome of temperature elevation on MPXV infection remains poorly defined. We isolated a circulating strain of MPXV from a patient who presented with fever (38.5 °C) and rash from the 2022 outbreak. Genomic sequencing identified this isolate to belong to the epidemic Clade IIb.B1. Transcriptomic analysis demonstrated this virus strain to induce a strong IL6 pro-inflammatory immune response, consistent with a role for this pyrogen in the regulation of fever. We identify basal host-cell temperature at both physiological and febrile temperatures to be a key determinant in the outcome of MPXV infection that governs the differential regulation of viral transcription and amplitude of host response to infection. Incubation of infected tissues or cells at 38.5 or 40 °C led to a restriction or ablation in MPXV replication, respectively. Importantly, this thermal inhibition was entirely reversible upon temperature downshift to 37 °C. Co-stimulation of the type-I interferon (IFN) response led to a dose- and temperature-dependent inhibition in MPXV replication that restricted the re-establishment of infection upon thermal downshift. Collectively, our data identify febrile temperatures associated with mpox to be a key determinant in the outcome of infection that can synergise with the type-I IFN response to amplify the host-cell restriction of MPXV.

Introduction

MPXV belongs to the Orthopoxvirus (OPXV) genus[1], which includes variola virus (VARV, the causative agent of smallpox) and vaccinia virus (VACV, the foundation virus of the smallpox vaccine). Since January 2022, the World Health Organization (WHO) reported a global rise in the number of confirmed mpox cases across all six WHO regions (> 90,000 confirmed cases and ≥ 150 deaths; September 2023), including previous non-endemic regions of Europe and the Americas (https://worldhealthorg.shinyapps.io/mpx_global/). While the natural zoonotic reservoir of MPXV is likely to be in small rodents[2-4], increased human-to-human transmission has been widely reported during the 2022/23 outbreak and linked to the emergence of Clade IIb variants since 2016[5-7]. This has raised concern that MPXV may

64 establish a global foothold in the human population due to waning levels of cross-protecting
65 immunity conferred previously through smallpox vaccination[8,9].
66 Human-to-human transmission of MPXV occurs through close contact with infectious
67 skin lesions, bodily fluids, or large respiratory droplets[3,4]. The spectrum of mpox disease is
68 often variable and ranges from self-limiting disease in healthy immunocompetent adults to
69 fatality in 1 to 10 % of affected individuals[10]. Common prodrome symptoms include fever,
70 lymphadenopathy, pharyngitis, headache, and myalgia, followed by rash and skin lesions on
71 the body, face, and genitals[8,10-13]. More than 70 % of confirmed cases result in fever, with a
72 reported febrile temperature range of 38.3 to 40.5 °C[11,14-17]. Fever is an evolutionary
73 conserved host response to infection and inflammation that can influence multiple cellular
74 processes, including host immunological responses to infection[18,19]. Body temperature varies
75 throughout the day, with age, sex, and ethnic origin being contributing factors[20,21]. Unlike
76 heat stroke or hyperthermia, fever represents a controlled shift in body temperature activated
77 in response to exogenous (microbial) and endogenous (host) pyrogenic factors[20-22]. Clinical
78 febrile temperatures can vary (ΔT of 1 to 4 °C above baseline); with low (38 to 39 °C),
79 moderate (39.1 to 40 °C), high (40.1 to 41 °C), and hyperpyrexia (> 41.1 °C) temperature
80 ranges[21]. Experimental evidence has shown tissue temperature to play a key role in
81 regulating viral infection and the induction of interferon (IFN)-mediated antiviral innate
82 immune defences to infection[23-26]. Notably, antipyretic treatment of intensive care patients
83 infected with influenza A virus (IAV) has been linked to increase patient mortality[27-29],
84 suggesting a beneficial role of the fever response to protect against infection in a clinical
85 setting.
86 While small animal and non-human primate (NHP) models have shown MPXV
87 infection to induce fever[30-32], few studies have directly examined the influence of temperature
88 on the outcome of infection. Historical evidence (circa 1960s) has shown divergent OPXVs
89 to have variable ceiling temperatures of pox formation in chick embryos, with mpox
90 restriction observed at temperatures ≥ 39.5 °C[33,34]. These findings suggest that temperature
91 elevation is likely to play a key determinant in the replication and/or immunopathology of
92 MPXV. However, *in vitro* studies have focused on laboratory-adapted strains of VACV,
93 which are known to carry strain-specific mutations that can influence their thermal- and/or
94 immuno-regulatory properties[22,35-38]. Thus, the influence of temperature elevation to control
95 the outcome of OPXV infection remains poorly defined, specifically in circulating Clades or
96 strains of human origin. We therefore set out to investigate the net effect of temperature

97 elevation on the replication of MPXV using a clinical isolate derived from the 2022/23
98 outbreak.
99 We isolated a circulating strain of MPXV from a febrile hospitalised patient during
100 the 2022 outbreak. Genomic sequencing demonstrated this isolate belonged to the Clade
101 IIb.B1 epidemic strain. We demonstrate basal host-cell temperature to be a key determinant
102 in the outcome of MPXV infection at both physiological skin temperature (33 °C) and febrile
103 (38.5 and 40 °C) temperatures relative to core body temperature (37 °C). Incubation of
104 infected cells at 40 °C led to an ablation in MPXV replication. We show this thermal
105 restriction to occur via a genome wide suppression in viral transcription, with multiple viral
106 open reading frames (vORFs) displaying temperature-dependent profiles of differential gene
107 expression (DEG). Importantly, we show that the thermal restriction of MPXV is reversible
108 upon temperature downshift to 37 °C. Co-stimulation of the type-I IFN response led to a
109 dose- and temperature-dependent IFN-mediated restriction in MPXV replication that
110 attenuated the re-establishment of infection upon thermal downshift. Our data identify a
111 cooperative and synergistic role for temperature elevation to enhance the type-I IFN-
112 mediated restriction of MPXV. Findings pertinent to the immunological regulation of many
113 clinical pathogens that induce a fever response.
114

115 ## Results

116 **Temperature elevation inhibits MPXV replication in a cell-type dependent manner.**
117 We isolated a clinical strain of MPXV from a PCR positive patient presenting with fever
118 (38.5 °C) and rash. Illumina sequencing of inactivated clinical swabs (CVR_MPXV1a) and
119 infectious cell culture supernatant derived from primary amplification (MPXV CVR_S1)
120 identified an identical MPXV genome (accession number ON808413) (Fig 1A). Phylogenetic
121 analysis identified this virus to belong to the MPXV Clade IIb.B1 lineage and to contain 67
122 single nucleotide polymorphisms (SNPs) compared to the MPXV Clade II reference strain
123 (NC_063383). SNPs were located across the genome and present in both core and accessory
124 vORFs. Consistent with previous MPXV Clade IIb genomic analysis[7,39,40], 91% of the
125 identified SNPs (61 out of 67 nucleotides) were consistent with APOBEC deamination (G to
126 A or C to T substitutions; Fig 1B).
127 As MPXV CVR_S1 (here after referred to as MPXV) was isolated from a patient with
128 fever, we next investigated the influence of tissue temperature on MPXV replication in skin
129 epithelium. Human keratinocytes were differentiated into a pseudostratified epithelium under

130 air liquid interface (ALI). Tissues were mock treated or infected with MPXV (10^2 or 10^3
131 plaque-forming units (PFU)/tissue) at 37 °C for 1 h prior to continued incubation at 33, 37, or
132 40 °C (representative of skin, core, and maximum febrile temperature range, respectively) for
133 72 h. Haematoxylin and eosin (H&E) staining of mock treated tissue sections demonstrated
134 no significant difference in skin epithelium thickness, morphology, or integrity over the
135 temperature range of incubation (Fig 2A, B; Fig S1). As expected, immunohistochemistry
136 (IHC) staining of tissue sections identified MPXV virion antigen expression to increase in a
137 multiplicity of infection (MOI) dependent manner at 37 °C (Fig 2A; Fig S1). Notably,
138 discrete foci of infection could be observed at both 33 and 37 °C under low MOI (10^2
139 PFU/tissue), indicative of MPXV intraepithelial propagation and spread. Quantitation of
140 immunohistochemistry (IHC) stained tissue sections demonstrated the relative levels of
141 MPXV infection to be dependent on incubation temperature, with the highest levels of
142 replication observed at 37 °C (Fig 2C, D). Importantly, a significant reduction in MPXV
143 staining could be observed at both physiological (37 *vs*. 33 °C) and febrile (37 *vs.* 40 °C)
144 incubation temperatures, with MPXV staining at 40 °C close to background levels observed
145 in mock treated samples (Fig 2C, D). Together, these data identify tissue temperature to play
146 a key determinant in the outcome of MPXV replication at both physiological and febrile
147 temperature ranges associated with clinical infection.
148 To examine the influence of temperature on the replication kinetics of MPXV in more
149 detail, we next compared the thermal sensitivity of MPXV to that of VACV (strain WR;
150 internal positive control)[38]. Human foreskin fibroblast (HFt) cells were infected at 37 °C for 1
151 h prior to incubation at 33, 37, 38.5 or 40 °C (representative of skin, core, and low to
152 moderate grade febrile temperature ranges, respectively). Infected monolayers were fixed at
153 48 h and analysed for viral plaque formation by Coomassie staining. Consistent with previous
154 results[38], VACV demonstrated a significant decrease in plaque number, plaque size, and titre
155 of cell-released virus (CRV) at incubation temperatures > 37 °C (Fig 3A to D). Notably,
156 plaque formation could still be observed at 40 °C, demonstrating the inhibitory ceiling
157 temperature for VACV had yet to be reached (Fig 3A, B)[38]. A significant reduction in plaque
158 size and CRV titre could also be observed upon incubation at 33 °C (Fig 3A to D),
159 demonstrating physiological temperatures below 37 °C to be inhibitory to optimal VACV
160 replication. qPCR analysis of intracellular viral DNA (vDNA) levels harvested at 2 h post-
161 infection (hpi; 1 h post-temperature shift) demonstrated the thermal restriction of VACV to
162 occur independently of a block to virus entry (Fig 3E). Moreover, no significant difference in
163 cell number, cell viability, or puromycin-induced cell death was detected in mock treated

164 cells at 40 °C relative to incubation at 37 °C (Fig S2A, B), confirming cell monolayer health
165 and responsiveness to stimuli at temperatures > 37 °C. These data validate our experimental
166 model system and corroborate VACV to be sensitive to thermal restriction at temperatures ≥
167 38.5 °C[38]. Analogous infections demonstrated MPXV plaque formation and plaque size to be
168 highly sensitive to alterations in incubation temperature, with reduced numbers of plaques
169 observed at 33 °C, reduced plaque size at 38.5 °C, and a complete inhibition in viral plaque
170 formation at 40 °C (Fig 3F to H). Significantly lower titres of CRV were also detected at 33,
171 38.5, and 40 °C relative to incubation at 37 °C independently of a block to virus entry (Fig 3I,
172 J). To establish whether the temperature-dependent restriction observed in OPXV replication
173 was a consequence of a failure of HFt cells to support DNA virus replication, we examined
174 the plaque formation of herpes simplex virus 1 (HSV-1, strain 17syn+) over an equivalent
175 temperature range. Only a modest restriction in plaque count was observed at 40 °C (Fig
176 S2C), demonstrating HFt cells to support viral DNA replication over a wide range of
177 incubation temperatures. Thus, we identify a low-passage MPXV clinical isolate to be
178 sensitive to thermal restriction at both physiological (33 °C) and febrile (38.5 or 40 °C)
179 temperatures relative to incubation at core body temperature (37 °C).
180 As MPXV is known to infect a wide variety of cell types *in vivo*[30], we investigated if
181 the thermal sensitivity of either VACV or MPXV occurred in a cell-type dependent manner.
182 Infection of human normal oral keratinocytes (NOK) and retinal pigmented epithelial (RPE)
183 cells with VACV demonstrated an equivalent trend in thermal restriction to that observed in
184 HFt cells (Fig 4A, B, Fig S2D). Notably, infection of *Chlorocebus sabaeus* or *Chlorocebus*
185 *aethiops* (African green monkey) kidney derived epithelial or fibroblast cells (Vero E6 and
186 CV-1 cells, respectively) demonstrated significantly higher levels of VACV plaque formation
187 at 33 °C relative to incubation at 37 °C (Fig 4A, B, Fig S2D). These data demonstrate that the
188 thermal permissivity of cells to support VACV replication to be cell-type dependent.
189 Analogous infection with MPXV demonstrated distinct cell-type dependent profiles of
190 thermal restriction at 33 °C (HFt, RPE, and CV-1 cells) and 38.5 °C (NOK, Vero E6, and
191 CV-1 cells) relative to infection and incubation at 37 °C (Fig 4C, D, Fig S2E). All cell lines
192 demonstrated a complete, or near complete (CV-1 cells), restriction in MPXV plaque
193 formation at 40 °C (Fig 4C, D). We conclude the basal and ceiling temperatures that support
194 or restrict MPXV replication to be cell-type dependent.
195

196 **Basal host-cell temperature differentially regulates the outcome of MPXV transcription.**
197 To determine where the block in MPXV replication might occur, we performed RNA
198 sequencing (RNA-Seq) on mock treated or MPXV infected HFt cells incubated at 33, 37,
199 38.5 or 40 °C (MOI 0.01 PFU/cell, 48 h). Transcriptome analysis of 24 reference genes
200 known to be expressed across a wide range of tissues and cell-types[41-43] demonstrated no
201 significant difference in their relative profile of expression in mock treated cells across the
202 temperature range of analysis (Fig S3A). Moreover, no significant difference was observed in
203 the total number of host mapped read (MR) counts derived from mock treated samples across
204 the temperature range (Fig S3B, grey bars). These data indicate host-cell transcription to
205 remain largely unperturbed in mock treated cells up to 40 °C. In contrast, a significant
206 difference in host MR counts was observed in MPXV infected cells incubated at 33, 37, and
207 38.5 °C relative to mock treatment at 37 °C (Fig S3B, green bars). No significant difference
208 in host MR count was observed between MPXV infected cells incubated at 40 °C and mock
209 treatment at 37 °C. These data indicate MPXV infection to significantly influence the
210 outcome of host transcription at incubation temperatures permissive to MPXV replication
211 (Fig 3F to I). Investigating further, principal component analysis (PCA) of viral MR counts
212 identified febrile temperatures (38.5 and 40 °C) to have the highest degree of variance in viral
213 transcript abundance relative to infection at 37 °C (Fig 5A). Analysis of vORF MR counts
214 identified infected cells incubated at 40 °C to have suppressed levels of MPXV transcription
215 (Fig 5B, C, Fig S3C). Notably, the overall profile of transcription remained proportionate
216 between incubation temperatures, with an approximate 1000-fold reduction in transcript
217 levels per vORF at 40 °C relative to incubation at 37 °C (Fig 5B, C, Fig S3C). Seven vORFs
218 were identified to have values below 10 MR counts (Fig 5B, purple circles and text). Of
219 these, four vORFs (gp039, gp083, gp120, gp135) encode proteins involved in intracellular
220 virus maturation, one virus toll like receptor (vTLR; gp024) implicated in immune
221 antagonism, and one subunit of the vRNA polymerase complex (gp069) (Fig 5D, purple text;
222 Fig S3D). Thus, we attribute the ablation of MPXV replication at 40 °C to suppressed levels
223 of viral transcription which bottleneck or restrict the progress of infection. As we had
224 observed a significant difference between viral MR counts at lower incubation temperatures,
225 we next compared transcription profiles derived from MPXV infected cells incubated at 33
226 and 38.5 °C. Relative to 37 °C (Fig 5E, solid grey line), distinct profiles of MPXV
227 transcription could be observed between these two incubation temperatures. Notably, many
228 vORFs displayed opposing viral MR count profiles of transcript expression (Fig 5E, dotted
229 grey ellipses). Five functionally unrelated vORFs (gp007, gp146, gp147, gp148, gp150) were

230 identified to be significantly downregulated at 33 °C (≥ 1.5 log2 FC) relative to incubation at
231 37 °C (Fig 5E, orange circles and text; Fig S3E). We conclude basal host-cell temperature to
232 play a key determinant in the differential regulation of MPXV transcription at both
233 physiological skin temperature (33 °C) and febrile (38.5 or 40 °C) temperatures relative to
234 infection at core body temperature (37 °C). Collectively (Figs 2 to 5), these data identify the
235 optimal temperature for MPXV Clade IIb.B1 replication to be 37 °C.
236
237 **Basal temperature differentially regulates the host-cell response to MPXV infection.**
238 As we had identified temperature to differentially regulate MPXV transcription (Fig 5), we
239 next investigated the influence of temperature on the host-cell response to infection. We
240 performed RNA-Seq analysis on mock treated or MPXV infected HFt cells incubated at 33,
241 37, 38.5 or 40 °C (MOI 0.01 PFU/cell, 48 h). Pairwise comparisons identified unique and
242 shared clusters of DEGs (FDR < 0.05, ≥ 1.5 log2 FC) across the temperature range of
243 analysis (Fig 6A, B). Relatively few DEGs were identified between mock treated and
244 infected samples incubated at 40 °C, suggesting MPXV infection at this temperature to
245 induce a minimal host-cell response (Fig 6A, B; yellow ellipses and lines). This was
246 surprising, as we had observed equal levels of MPXV genome entry into infected cells across
247 the temperature range of analysis (Fig 3J). These data identify the onset of MPXV replication
248 to be a key determinant in the host-cell response to infection. Pathway analysis identified
249 distinct profiles of DEG enrichment dependent on incubation temperature, with 33 and 38.5
250 °C sharing the highest degree of similarity in their respective host-cell responses to infection
251 (Fig 6C, grey lines). Notably, many pathways were only significantly enriched in response to
252 infection at 37 °C (Fig 6C), even though cells incubated at 33 and 38.5 °C were observed to
253 be productively infected and to be releasing infectious virus (Figs 2 to 4). These data
254 demonstrate basal host-cell temperature to play a key role in the outcome and/or amplitude of
255 host-cell response to MPXV infection. Consistent with this finding, we observed multiple
256 cytokine-related pathways to be differentially regulated in response to MPXV infection (Fig
257 6C, black arrows). Analysis of these DEGs (71 genes in total) revealed distinct profiles of
258 immune gene expression that were dependent on both infection and incubation temperature
259 (Fig 6D to F). Importantly, this host-cell immune response to infection occurred
260 independently of the induction of the type-I IFN response (Fig 6G, Fig S4A, B). While
261 *IFNB1* was identified to be a DEG (Fig 6G, black arrow), levels of *IFNB1* expression were
262 extremely low (MPXV 37 °C mean CPM = 0.1285, -/+ 0.02 SD; Fig S4A, B), with little to

263 no significant change observed in the overall profile of host interferon responsive genes
264 (IRGs; Fig S4C, D). These data demonstrate Clade IIb.B1 MPXV infection to effectively
265 suppress the induction of IFN-mediated antiviral immune defences. Notably, MPXV infected
266 cells incubated at 40 °C expressed an equivalent cytokine profile to that of mock treated
267 samples across the temperature range of analysis (Fig 6D, E [purple arrow], Fig S4E). Thus,
268 viral genome entry into host-cells alone is not sufficient to trigger the activation of pathogen
269 recognition receptors (PRRs) necessary for the induction of cytokine-mediated pro-
270 inflammatory immune responses to infection. Collectively, these data demonstrate MPXV to
271 induce a temperature-dependent cytokine response to infection that requires the onset of
272 productive lytic replication.
273 Investigating further, we compared the host-cell transcriptome profiles of MPXV
274 infected cells incubated at 37 and 40 °C. Out of the 935 DEGs (FDR <0.05, ≥ 1.5 log2 FC)
275 identified (Fig 7A), pathway analysis identified cell cycle (Fig 7B, grey arrow and circle) and
276 immune system (Fig 7B, coloured arrows and circles) pathways to be significantly
277 downregulated at 40 °C relative to incubation at 37 °C (Fig 7B). Analysis of immune system
278 related DEGs (61 genes in total) identified signalling by interleukin (IL; 20 DEGs) and
279 adaptive immune system (21 DEGs) pathways to account for the majority of DEGs identified
280 between these two infection conditions (Fig 7C, D). In contrast to IFN signalling (Fig S4A to
281 D), analysis of the IL signalling pathway (R-HAS-449147; 459 genes in total) identified this
282 pathway to be significantly upregulated during MPXV infection in a temperature-dependent
283 manner (Fig 7D green dots, Fig S4F). Notably, multiple cytokines and chemokines
284 implicated in IL signalling were observed to vary in their relative profiles of expression
285 between 33 and 38.5 °C (Fig 7E; e.g., IL12A [$P = 0.0026$], CXCL8 [$P = 0.0001$]).
286 Importantly, MPXV incubation at 40 °C failed to upregulate these cytokine-related genes
287 above baseline levels (Fig 7D, E, Fig S4E, F). Together, these data demonstrate MPXV to
288 induce a robust IL response to infection in a temperature-dependent manner.
289
290 **Basal temperature differentially regulates the host-cell IFN response to MPXV**
291 **infection.**
292 As the IFN response is known to play a significant role in limiting OPXV pathogenicity and
293 immune clearance[44,45], we next investigated whether basal host-cell temperature influenced
294 the IFN-mediated host-cell restriction of MPXV infection. HFt cells were stimulated with
295 IFN-β and incubated at 33, 37, 38.5 or 40 °C for 16 h prior to MPXV infection (MOI 0.001

296 PFU/cell) and continued incubation in the presence of IFN for 48 h at their respective
297 temperatures. Quantitation of plaque counts demonstrated MPXV restriction to occur in an
298 IFN-β dose- and temperature-dependent manner, with heightened levels of restriction
299 observed at 38.5 °C relative to incubation at 33 or 37 °C (Fig 8A to D). Consistent with our
300 previous analysis (Figs 2 to 4), MPXV plaque formation was abrogated at 40 °C irrespective
301 of IFN stimulation (Fig 8A, B grey dotted lines and circles). IFN pre-treatment and infection
302 with VACV demonstrated an analogous dose- and temperature-dependent trend in VACV
303 restriction (Fig S5A to D). Together, these data identify temperature elevation to cooperate
304 with the type-I IFN response to mediate the host-cell restriction of MPXV. As temperature
305 elevation alone led to suppressed levels of MPXV transcription independently of the
306 induction of the type-I IFN response (Figs 5, 6, S4A to D), we next investigated the
307 synergistic nature of temperature elevation and IFN co-stimulation on the outcome of MPXV
308 infection. Naïve HFt cells were infected with MPXV (MOI 0.01 PFU/cell) for 1 h at 37 °C
309 prior to overlay with IFN-β and incubation at 33, 37, 38.5 or 40 °C. Infected cell monolayers
310 were fixed at 24 hpi and the number of MPXV virion antigen positive cells quantified by
311 immunostaining. Consistent with our IHC analysis (Fig 2), incubation temperature
312 dramatically reduced the number of MPXV antigen positive cells detected at 24 hpi (Fig 8E,
313 F no IFN; 37°C > 33 ≈ 38.5 °C > 40 °C). Notably, a substantial number of MPXV antigen
314 positive cells could still be detected at 40 °C, indicating that a proportion of MPXV genomes
315 were able to circumvent complete thermal restriction (Fig 8E, F no IFN). Co-stimulation
316 with IFN-β led to a dose- and temperature-dependent reduction in the number of MPXV
317 antigen positive cells (Fig 8E, F plus IFN). These data demonstrate temperature elevation and
318 the type-I IFN response to act cooperatively in the host-cell restriction of MPXV. As neither
319 temperature elevation nor IFN stimulation was sufficient to eliminate MPXV gene expression
320 (either alone or in combination), we hypothesised MPXV replication may recover following
321 temperature downshift to 37 °C and/or washout of IFN as an immune stimulus. Downshift of
322 infected cells from 40 (no IFN treatment) to 37 °C led to a complete recovery in MPXV
323 plaque formation to equivalent levels observed at 37 °C (Fig 8G). These data demonstrate
324 MPXV thermal restriction to only stall the progress of infection, as opposed to eliminate or
325 induce the establishment of viral genome quiescence. Surprisingly, IFN washout from
326 infected and IFN treated cells incubated at 37 °C also led to an equivalent recovery in MPXV
327 plaque formation (Fig 8H). Analogous to temperature restriction, these data demonstrate the
328 type-I IFN response to suppress, but not eliminate, MPXV infection. Importantly, IFN

329 washout and thermal downshift of MPXV infected and IFN stimulated cells from 40 to 37 °C
330 led to a significantly lower recovery in the re-establishment of MPXV infection in an IFN
331 dose-dependent manner compared to analogous samples incubated at 37 °C (Fig 8J).
332 Equivalent trends in the re-establishment of infection were also observed following IFN
333 washout and temperature downshift of VACV infected cells (Fig S5G to J). Thus, we
334 conclude temperature elevation to synergise with and enhance the type-I IFN-mediated
335 restriction of MPXV to limit the re-establishment of infection upon host-cell recovery from
336 these two independent pro-inflammatory immune responses known to be activated in
337 response to infection *in vivo*[32,46].
338

339 **Discussion**

340 The emergence of novel MPXV Clade IIb variant strains that support heightened levels of
341 human-to-human transmission is a global health concern and highlights the need for a better
342 understanding of MPXV and its interaction with the host immune system. The pro-
343 inflammatory fever response is a well-established and common prodrome symptom of
344 MPXV infection[11,14-17], but the precise thermoregulatory impact on the outcome of infection
345 has remained poorly defined. Here, we isolated a clinical Clade IIb.B.1 MPXV strain (MPXV
346 CVR_S1) from a hospitalised patient admitted with fever (38.5 °C) to determine the
347 influence of temperature elevation on the outcome of MPXV infection.
348 Previous studies (circa 1960s) have shown OPXVs to have divergent ceiling
349 temperatures of pox formation in the chorioallantoic membrane of infected embryonic
350 chicken eggs, ranging from 38 °C to ≥ 40.5 °C (VARV minor to VACV, respectively)[33,34].
351 Here we show the clinical febrile temperature range of 38.5 to 40 °C, representative of low-
352 to moderate-grade fever in humans[11,14-17,21], to restrict the replication of a circulating MPXV
353 Clade IIb strain. This temperature-dependent restriction was observed across a variety of
354 infection models (Figs 2 to 4), including pseudostratified skin epithelium, and is consistent
355 with the reported ceiling temperature of MPXV pox formation in embryonic chicken eggs of
356 39.5 °C[33]. Collectively, these data demonstrate that febrile temperatures associated with
357 mpox disease in humans may be a key determinant in the outcome of infection. Importantly,
358 we show that the thermal restriction of MPXV to occur independently of a block to virus
359 entry (Fig 3J) and to be reversible upon temperature downshift without impairment to viral
360 replication fitness (Fig 8G). These findings are consistent with the re-establishment of VARV
361 replication in embryonic chicken eggs upon thermal downshift from its inhibitory ceiling

362 temperature of 38.5 °C[34]. As OPXVs with alternate ceiling temperatures have been shown to
363 complement quiescent infections leading to hybrid pox formation[34,47], variance in MPXV
364 Clade and strain ceiling temperatures might contribute to genetic reassortment during mixed
365 co-infection and/or changes in viral pathogenesis. Thus, the thermoregulatory mechanisms
366 surrounding MPXV genome stability, longevity, and retention of replication fitness at febrile
367 temperatures warrants further investigation. Importantly, we demonstrate lower physiological
368 temperatures associated with skin tropism to also impact on MPXV replication. We observed
369 a significant reduction in MPXV intraepithelial propagation, plaque formation, and virus
370 yield following incubation at 33 °C (Figs 2 to 4). We posit the fever response to both
371 positively and negatively influence the outcome of OPXV infection dependent on the
372 baseline temperature of the tissue at the point of infection. For example, a general two to four
373 °C rise in skin temperature from 33 to 37 °C would be expected to promote MPXV
374 replication, whereas a similar rise in tissue temperature from 37 °C we show to be
375 progressively inhibitory (Figs 2 to 4). Thus, inherent differences in species body/tissue
376 temperature and/or capacity to mount a febrile immune response could impact on the
377 zoonotic potential of MPXV to be maintained within an animal reservoir or to undergo inter-
378 species host transmission. Indeed, available evidence suggests small rodent models to have
379 variable febrile responses to OPXV infection, potentially in an MPXV Clade dependent
380 manner[22,30-32]. Thus, the influence of tissue temperature on MPXV species tropism and
381 onward transmission also warrants additional investigation.
382 Our transcriptomic analysis demonstrates host-cell temperature to have a significant
383 impact on the differential regulation of viral transcription and associated host-cell responses
384 to MPXV infection, both at physiological (33 °C) and febrile (38.5 and 40 °C) temperatures
385 relative to core body temperature (37 °C; Figs 5 to 7). MPXV incubation at 40 °C led to a
386 substantial decrease in viral transcription (≈ 1000-fold decrease in MR count per vORF; Fig
387 5B, C). However, the overall profile of transcription remained proportionate to that observed
388 at 37 °C (Fig 5B), indicative of a genome-wide suppression in transcription, as opposed to a
389 specific block in the expression of any individual vORF. These data complement our qPCR
390 analysis (Fig 3J), which collectively demonstrate incubation temperature not to inhibit
391 MPXV genome entry or the initiation of viral transcription upon primary infection. Notably,
392 we identify multiple vORFs that encode proteins associated with virion maturation (gp039,
393 gp083, gp120, and gp135) to show substantially decreased transcript levels (≤ 10 MR counts
394 per ORF; Fig 5B, D). Consistent with this observation, significantly lower levels of virion

395 antigen expression were also observed within MPXV infected tissues or cells incubated at 40
396 °C (Figs 2, 8E). Thus, temperature elevation is likely to cause a bottleneck in the expression
397 of critical viral gene products required for virion maturation that suppress the onward
398 propagation and spread of MPXV. Notably, differential patterns of MPXV transcription and
399 replication fitness were also observed at lower temperatures (Figs 2, 3, 4, 5E). Incubation at
400 33 °C led to a 50 % decrease in viral plaque formation, whereas incubation at 38.5 °C
401 resulted in a 50 % decrease in viral plaque size relative to incubation at 37 °C (Figs 3G, H,
402 4C). Together, these data highlight the importance of basal host-cell temperature to the
403 outcome of MPXV infection. We posit that the differential patterns of viral transcription
404 observed between 33 and 38.5 °C to account for the phenotypic differences identified
405 between these two incubation temperatures. Of the five vORFs identified to be significantly
406 downregulated at 33 °C (Fig 5E, orange circles), experimental evidence has shown the
407 VACV orthologues of gp148 (VACV A43R), gp007 (VACV D6L), and gp146 (VACV
408 A41L) to impact on viral replication fitness and lesion formation[48-51]. Thus, the differential
409 patterns of viral transcription observed at both physiological and febrile temperatures are
410 likely to effect multiple viral and cellular processes that govern the overall outcome of
411 infection.
412 Our host-cell transcriptome analysis of mock treated or MPXV infected cells
413 incubated at 40 °C identified relatively few DEGs (13 in total; Fig 6A, B) at this incubation
414 temperature. This minimal host-cell response correlates with the limited levels of MPXV
415 transcription and replication observed at 40 °C (Figs 2 to 5). Thus, viral genome entry into
416 host-cells alone is not sufficient to activate PRRs necessary to induce a pro-inflammatory
417 immune response to infection (Figs 6, S4). In contrast, we identify a significant induction of
418 pro-inflammatory interleukin gene expression at both physiological skin and core body
419 temperatures (33 and 37 °C, respectively) and febrile (38.5 °C) temperatures permissive to
420 MPXV replication. The differential patterns of IL and chemokine expression correlate well
421 with the levels of MPXV replication observed at these temperatures. For example, IL-6
422 induction (a key pyrogen in the regulation of the fever response)[52] demonstrated peak
423 induction at 37 °C, with lower levels of induction observed at 33 or 38.5 °C (Fig 7E),
424 consistent with decreased levels of replication observed at these incubation temperatures
425 (Figs 2, 3). Thus, we identify basal host-cell temperature to be a key determinant in the
426 amplitude of cytokine response to MPXV infection. These data are consistent with cytokine
427 profiling experiments of serum samples derived from experimentally infected NHPs or
428 hospitalised patients that have shown pro-inflammatory interleukin expression levels to

429 correlate with the kinetics of MPXV replication and disease severity, respectively[32,46]. While
430 MPXV encodes immune antagonists to IL-1 (gp014, gp152, gp167), IL-18 (gp007), TNF-α
431 (gp002, gp178), IFN-α/β (gp169), and IFN-γ (gp163), among others[44], it does not encode a
432 direct IL-6 antagonist. This raises the possibility that specific profiles of pro-inflammatory
433 cytokine or chemokine expression may be beneficial to MPXV replication prior to
434 temperature elevation, potentially through the recruitment, inactivation, and infection of
435 bystander and/or circulating immune cells[44].
436 The type-I IFN response is a critical component of the host's antiviral immune
437 defence, which acts to restrict viral propagation and to prime adaptive immune responses to
438 clear MPXV infection[44,45,53-55]. Due to their large coding capacity, OPXVs encode multiple
439 immune antagonists to block the induction of the type-I IFN response at several independent
440 stages of infection[44,45,56,57]. Correspondingly, we demonstrate a clinical MPXV IIb.B1 strain
441 to effectively inhibit the induction of the type-I IFN response (Figs 6, S4). Importantly, the
442 activation of PRRs that regulate the pro-inflammatory IFN response can be triggered through
443 multiple mechanisms, including the detection of damage-associated molecular patterns
444 (DAMPs) and pathogen associate molecular patterns (PAMPs). We posit the IFN signature
445 observed in response to MPXV infection *in vivo* is likely a consequence of DAMP activation
446 due to the high levels of replication observed in multiple cell-types and organs upon viral
447 dissemination[32,44,46]. We demonstrate a circulating MPXV IIb.B.1 strain to be sensitive to
448 exogenous IFN-β stimulation in a dose- and temperature-dependent manner (Fig 8). These
449 data are consistent with previous reports that have shown Clade I MPXV strains to be
450 sensitive to exogenous IFN stimulation at 37 °C[53,55]. Importantly, we demonstrate this IFN-
451 mediated restriction to be reversible and not to effectively eliminate infection, with
452 significantly lower levels of MPXV recovery observed at febrile temperatures associated with
453 clinical infection (Fig 8H, J). Thus, we identify functional similarity and synergism between
454 pro-inflammatory immune responses (fever plus IFN) that cooperate to mediate the
455 accumulative host-cell restriction of MPXV. Such accumulative effects are likely to be a
456 consequence of suppressed levels of viral transcription at febrile temperatures restricting the
457 ability of MPXV to express immune antagonists that directly counteract the effects of IFN
458 (e.g., the viral IFN-α/β receptor antagonist gp169)[56]. We posit that such cooperation between
459 pro-inflammatory immune responses will likely play a significant role *in vivo* to limit viral
460 propagation and to prime adaptive immune responses required to clear MPXV infection[54].

461 In conclusion, our study provides critical insights into the importance of temperature
462 in the regulation and outcome of MPXV infection. We identify host-cell temperature at both
463 physiological and febrile temperatures to be a key determinant in the regulation of viral
464 transcription, amplitude of host-cell cytokine response to infection, and ancillary interactions
465 with the IFN response required to inhibit MPXV replication. Our data shed light on the
466 complex interplay and functional synergy between host pro-inflammatory immune systems
467 and their associated outcomes to infection, findings pertinent to the immune regulation of
468 many clinical pathogens that induce a fever response.
469

470 ## Materials and Methods

471 **Cells and cell viability assays**

472 Vero E6 (a gift from Michelle Bouloy, Institute Pasteur, France), CV-1 (European Collection
473 of Authenticated Cell Cultures (EACC), 87032605), HFt[58], RPE-1 (ATCC, CRL-4000),
474 HaCaT (Addexbio, T0020001), and J2 3T3 (a gift from Sheila Graham, MRC-University of
475 Glasgow Centre for Virus Research) cells were grown in Dulbecco's Modified Eagle
476 Medium (DMEM; ThermoFisher, 10566016) supplemented with 10 % fetal bovine serum
477 (FBS; ThermoFisher 10270106) and 1 % penicillin streptomycin (PS; ThermoFisher,
478 15070063). NOK cells (a gift from Karl Munger, Tufts University School of Medicine,
479 USA)[59] were grown in Keratinocyte-SFM medium with L-glutamine, EGF, and BPE
480 (ThermoFisher, 17005075). All cells were grown and maintained at 37 °C in 5 % CO_2 unless
481 otherwise stated. Cell viability was measured using MTS reagent (Abcam, ab197010), as per
482 the manufacturer's guidelines, and absorbance measurements taken at OD=490 nm using a
483 PHERAstar plate reader (BMG LABTECH). As a positive control for cell death, puromycin
484 (Sigma-Aldrich, P8833) was added to cell culture media at a final concentration of 1.0 µg/ml
485 and incubated for 24 h prior to the addition of MTS.
486

487 **Organotypic raft culture**

488 Type I collagen was extracted from rat tails (supplied by the University of Glasgow,
489 Veterinary Research Facility). Ethanol sterilised tails were incubated in 0.5 M acetic acid at 4
490 °C for 48 hours on a magnetic stirrer. Material was clarified by centrifugation at 10,000 x g
491 for 30 minutes at 4 °C. Supernatant was subjected to collagen extraction by NaCl
492 precipitation (final concentration 10 % weight/volume) for 1 h at 4 °C and collected by
493 centrifugation at 10,000 x g for 30 minutes at 4 °C. The pellet was resuspended overnight in

494 0.25 M acetic acid and dialysis for three days (two changes per day) in pre-cooled acetic acid
495 (final concentration 17.4 mM) at 4 °C. Sterile collagen was isolated by centrifugation 20,000
496 x g for 2 h at 4 °C. Organotypic raft cultures were prepared as previously described[60]. Briefly,
497 collagen matrices with J2 3T3 fibroblasts were prepared in 12-well plates and allowed to
498 contract for approximately 7 days at 37 °C. Keratinocytes (HaCaT cells) were seeded on top
499 of contracted collagen matrices at a density of $2.5x10^5$ cells/matrix in 24-well plates and
500 incubated at 37 °C overnight prior to being transferred into Costar Transwells (Corning
501 Costar, 3401) and maintained at 37°C under air liquid interface (ALI) for 12 to 14 days.
502 Tissues were maintained in E-medium (3:1 ratio of DMEM:F12 (Thermofisher, 21765029)
503 medium supplemented with 10 % FBS and 1 % PS, 2 mM L-glutamine (ThermoFisher,
504 25030081), 180 µM adenine (Sigma-Aldrich, A2786), 5 µg/ml transferrin (Sigma-Aldrich,
505 T1147), 5 µg/ml insulin (Sigma-Aldrich, I6634), 0.4 mg/ml hydrocortisone (Sigma-Aldrich,
506 H0888), 0.1 nM cholera toxin (Sigma-Aldrich, C8052), and 0.2 ng/ml epidermal growth
507 factor (EGF; Sigma-Aldrich, E9644). Basal-chamber E medium was changed every 48 h.
508 Pseudostratified skin tissues were infected with 10^2 or 10^3 pfu/tissue (as indicated) in 50 µl
509 inoculum for 1 h at 37 °C prior to incubation at the indicated temperatures for 72 h.
510
511 **Immunohistochemistry**
512 Mock treated or infected pseudostratified skin epithelia was fixed in 8% (v/v) formaldehyde
513 overnight, washed in PBS, and processed by the Diagnostic Services, School of Biodiversity,
514 One Health and Veterinary Medicine, University of Glasgow. Following paraffin embedding,
515 3 µm sections were cut and placed in a 37 °C oven overnight. Samples were dewaxed in
516 HistoClear (National Diagnostics, HS-20) and rehydrated through 3x sequential washes in
517 ethanol (final concentration 70 %). Tissue sections were subject to antigen retrieval using
518 TET buffer (10 mM Tris base pH 9, 1 mM EDTA, 0.05% Tween-20) in a MenaPath access
519 retrieval unit at 125 °C and 15 psi for 100 sec, before cooling to room temp in H_2O and
520 transfer to TNET buffer (10 mM Tris pH 7.5, 100 mM NaCl, 1 mM EDTA, 0.05 % Tween-
521 20). Tissue sections were stained with a polyclonal antibody raised against whole VACV
522 (Invitrogen, PA1-7258; 1/2000 dilution) for 30 mins, washed in TNET buffer, prior to
523 secondary staining (Dako Envision polymer anti-rabbit, K4003) for 30 mins and washing in
524 TNET buffer. Visualisation was achieved using two 5 min applications of DAB+ (Dako,
525 K3468). Tissue sections were counterstained using Gills haematoxylin dehydrated, prior to
526 clearing in Histoclear, and mounting with a coverslip. Tissue sections were imaged using an
527 Aperio VERSA Digital Pathology Scanner (Leica Biosystem). Scanned tissue sections were

528 quantified using the Halo multiplex IHC module image analysis software (indica labs). The
529 algorithm was adapted for nuclei identification and arbitrary thresholds applied to detect
530 weak, moderate, and strong MPXV antigen positive cells over background levels of staining.
531 Algorithm optimisation was performed using the real-time Tuning function. All sections were
532 analysed using the same algorithm and subjected to random checks to confirm the precision
533 of tissue annotation.
534
535 **Viruses**
536 Clinical monkeypox virus (MPXV) CVR_S1 was isolated from an ISARIC4C patient with
537 ethical consent. The patient (44-year-old male) presented with fever, cough, myalgia, and
538 skin rash. Physiological admission parameters were temperature 38.5 °C, blood pressure
539 142/68, heart rate 96, oxygen saturation of 97 % on air, and respiratory rate of 18. Swabs
540 were collected from multiple skin lesions into virus transport medium (VTM). The VTM was
541 mixed in a 1:4 ratio with DMEM supplemented with 10 % FBS, 1 % PS and 250 ng/ml
542 Amphotericin B (ThermoFisher, 15290018) and centrifuged at 4000 rpm for 10 mins. Vero
543 E6 (sub-clone MESO; a gift from Meredith Stewart, MRC - University of Glasgow Centre
544 for Virus Research) cells were inoculated with 500 µl of VTM/media for 1 h. Infected
545 monolayers were washed three times in PBS prior to overlay with cell culture media and
546 incubation at 37 °C in the presence of 5 % CO_2. Media containing infectious cell-released
547 virus (CRV; primary amplification P1 stock) was harvested at 72 hours post-infection (hpi)
548 and clarified at 4000 rpm for 10 minutes. P1 virus was subjected to Illumina metagenomic
549 sequencing to evaluate purity and sequence homology to pre-culture clinical material
550 (CVR_MPXV1a; accession number ON808413) to confirm sequence identity and source of
551 the propagated isolate. All experiments were performed in a Biosafety level 3-laboratory at
552 the MRC-University of Glasgow Centre for Virus Research (SAPO/223/2017/1a). Vaccinia
553 Virus (VACV A5L-EGFP, a gift from Geoffrey Smith, University of Oxford, England)[61] was
554 propagated and titrated on Vero E6 (MESO) cells, as previously described[61,62]. Wild-type
555 herpes simplex virus 1 (HSV-1, strain 17syn+; a gift from Roger Everett, MRC - University
556 of Glasgow Centre for Virus Research) was propagated in RPE cells and titred on U2OS
557 cells, as previously described[63].
558

559 **Viral genome sequencing**

560 20 ng of nucleic acid was enriched for viral genomic sequences using NEBNext Microbiome
561 DNA Enrichment Kit (NEB, E2612) to reduce host genomic DNA contamination. Purified
562 DNA was sheared into 350-base pair fragments by sonication using the Covaris Sonicator
563 LE220. Library preparation was conducted with the KAPA Hyper kit (Roche, 07962347001)
564 with end repair and universal adapter ligation. Unique Dual Index Primer pairs (NEBNext
565 Multiplex Oligos for Illumina) were used to index the samples, followed by 10 cycles of PCR
566 amplification. Libraries were sequenced on the Illumina NextSeq500 platform with paired
567 ends for 2 x 150-base pair reads using a Mid-output cartridge Kit v2.5 (Illumina,
568 20024905). bcl2fastq software was used to demultiplex and compress bcl files into fastq (gz)
569 files. Sequence alignment was performed using MAFFT (v7.475)[64] and aligned to the MPXV
570 Clade IIa reference sequence (NC_063383.1). Variations between the sequences were plotted
571 using the Snipit program (v.1.1.2). APOBEC3-associated mutations (G=>A and C=>T) were
572 calculated from pairwise sequence alignment using a BASH script.

573

574 **Plaque and virus yield assays**

575 Cells were seeded onto plates and allowed to become confluent before infection at the
576 specified multiplicity of infection (MOI) for 1 h at 37 °C prior to overlay and incubation at
577 the indicated temperatures. For infectious cell-released virus (CRV) quantitation, harvested
578 supernatants were serially diluted in cell culture media and used as an inoculum to infect
579 Vero E6 (MESO) cells to obtain a linear range of countable plaques. Infected monolayers
580 were incubated at 37 °C for 24 to 72 h (dependent on the virus and experiment), fixed with 4
581 (VACV) or 8 (MPXV) % (v/v) formaldehyde (Sigma-Aldrich, F8775), washed in PBS, and
582 stained with 0.1 % Coomassie Brilliant Blue solution (Sigma-Aldrich, B0149) in 45 %
583 methanol and 10 % acetic acid for up to 30 minutes. Plates were washed in water and dried
584 overnight before plaque counting under a plate microscope. For quantitation of plaque
585 diameters, infected cell monolayers stained with Coomassie Brilliant Blue were imaged using
586 a Celigo Imaging Cytometer (Nexcelom Bioscience, UK) and plaque measurements
587 performed using Zen Blue software (Zeiss).

588

589 **Temperature and Interferon (IFN) inhibition assays**

590 Cells were infected at 37 °C for 1 h at the indicated MOI prior to overlay and continued
591 incubation at the desired temperature (33, 37, 38.5, or 40 °C) in 5 % CO_2 for the indicated

592 times prior to fixation and Coomassie Brilliant Blue or indirect immunofluorescence staining.
593 For IFN inhibition assays, cell monolayers were either pre-treated with IFN-β (R&D systems,
594 8499-IF-010; 0.1 to 200 IU/ml, as indicated) for 16 h at the indicated temperatures prior to
595 infection or infected for 1 h at 37 °C prior to the addition of IFN-β to the overlay and
596 incubation at the desired temperature (as indicated). For temperature downshift and IFN
597 washout experiments, duplicate infected plates were overlayed with media containing IFN-β
598 (0 to 200 IU/ml; as indicated) for 24 or 48 h (VACV or MPXV, respectively) prior to either
599 fixation or IFN washout (3x 1 ml cell culture media) and continued incubation at 37 °C for
600 24 or 48 h prior to fixation and Coomassie staining.
601
602 **Indirect immunofluorescence**
603 Mock treated, infected, or infected and IFN treated cells were fixed with 4 (VACV) or 8
604 (MPXV) % (v/v) formaldehyde, washed in PBS, and permeabilised with 0.5 % Triton-X-100
605 (Sigma-Aldrich, T-9284) prior to blocking in filter sterilised PBS containing 2 % FBS
606 (PBSf). Cells were stained with a polyclonal antibody raised against whole VACV
607 (Invitrogen, PA1-7258; 1/2000 dilution) and secondary staining using a donkey anti-rabbit
608 AlexaFluor 555 (Invitrogen, A31572). Cell nuclei were stained with DAPI (Sigma-Aldrich,
609 D9542). PBSf was used for all antibody incubations (1 h at RT) and cell washing throughout.
610 Cell monolayers were imaged and analysed using a Celigo Imaging Cytometer and
611 companion software (Nexcelom Bioscience, UK).
612
613 **Quantitative PCR**
614 PCR was carried out using NEB Luna Universal Probe One-Step RT-qPCR Kit according to
615 the manufactures' instructions (New England Biolabs, E3006). VACV was detected using
616 primers and probe directed to ORF E9L[65]; E9L forward primer: 5'-
617 CGGCTAAGAGTTGCACATCCA-3', E9L reverse primer: 5'-
618 CTCTGCTCCATTTAGTACCGATTCT-3' and E9L Probe 5'-
619 [6FAM]AGGACGTAGAATGATCTTGTA[BHQ1]-3'. MPXV was detected using the
620 primers and probe directed against the ORF G2R[66]; G2R FWD: 5'-
621 GGAAAATGTAAAGACAACGAATACAG-3', G2R REV 5'-
622 GCTATCACATAATCTGGAAGCGTA-3' and G2R Probe 5'-
623 [6FAM]AAGCCGTAATCTATGTTGTCTATCGTGTCC[BHQ1]-3'. 5 µl of extracted DNA
624 was used per 20 µl reaction and thermal cycling was performed on an Applied Biosystems

625 7500 Fast PCR instrument running SDS software v2.3 (ThermoFisher Scientific) under the
626 following conditions: 95 °C for 5 mins, followed by 45 cycles of 95 °C for 10 s and 62 °C for
627 30 mins.
628
629 **Viral entry assays**
630 HFt cells were seeded in 6-well plates at a cell density of $4x10^5$ cells/well 24 h prior to
631 infection. Cells were infected with MPXV or VACV at a MOI 0.1 PFU/cell for 1 h at 37 °C
632 before continued incubation at the desired temperature (as indicated) for a further 1 h. Cell
633 monolayers were washed twice in PBS before being trypsinised. Cells were pelleted at 3000
634 rpm for 5 mins and resuspended in 200 µl PBS. Total DNA was extracted using QIAamp
635 DNA kit (Qiagen, 51304), according to the manufacturer's instructions, with a final elution
636 volume of 20 µl. Viral genome levels were quantified by qPCR using virus specific primer
637 probe sets (described above) and normalised to GAPDH using an Applied Biosystems
638 FAM/MGB probe mix (Thermofisher, 4333764F).
639
640 **RNA sequencing (RNA-Seq)**
641 HFt cells were seeded onto 12-well plates at a density of $2x10^5$ cells/well. 24 h post-seeding,
642 cells were mock treated or infected with MPXV CVR_S1 (MOI 0.01) for 1h at 37 °C before
643 overlay and continued incubation at 33, 37, 38.5 or 40 °C (as indicated). Cells were washed
644 three times in PBS at 48 h prior to RNA extraction using a RNeasy plus Micro Kit (Qiagen,
645 74034). Eluted RNA was quantified using Qubit Fluorometer 4 (ThermoFisher, Q33238),
646 Qubit RNA HS Assay (Life Technologies, Q32855) and dsDNA HS Assay Kits
647 (ThermoFisher, Q32854) and quality controlled on a 4200 TapeStation System (Agilent
648 Technologies, G2991A) with a High Sensitivity RNA Screen Tape assay (Agilent
649 Technologies, 5067-5579). All samples had a RIN score of ≥ 8.8. 220 ng of total RNA was
650 used to prepare libraries for sequencing using an Illumina TruSeq Stranded mRNA Library
651 Prep kit (Illumina, 20020594) and SuperScript II Reverse Transcriptase (Invitrogen,
652 18064014) according to the manufacturer's instructions. Dual indexed libraries were PCR
653 amplified, purified using AgencourtAMPure XP magnetic beads (Beckman Coulter,
654 10136224), quantified using Qubit Fluorometer 4 (TheroFisher, Q33238) and Qubit dsDNA
655 HS Assay Kit (ThermoFisher, Q32854), and the size distribution assessed using a 4200
656 TapeStation System (Agilent Technologies, G2991A) with a High Sensitivity D1000 Screen
657 Tape assay (Agilent Technologies, 5067-5584). Libraries were pooled in equimolar
658 concentrations and sequenced using an Illumina NextSeq 500/550 sequencer (Illumina, FC-

659 404-2005). At least 95% of the reads generated presented a Q score of ≥ 30. RNA-Seq reads
660 were quality assessed using FastQC
661 (http://www.bioinformatics.babraham.ac.uk/projects/fastqc). Sequence adaptors removed
662 using TrimGalore (https://www.bioinformatics.babraham.ac.uk/projects/trim_galore/). RNA-
663 Seq reads were aligned to the *Homo sapiens* genome (GRCh38), downloaded via Ensembl
664 using HISAT2. HISAT2 is a fast and sensitive splice aware mapper, which aligns RNA
665 sequencing reads to mammalian-sized genomes using FM index strategy[67]. FeatureCounts[68]
666 was used to calculate mapped read counts that were normalized to counts per million (CPM;
667 unless otherwise stated). Generalized linear models (GLMs) with multi-factor designs was
668 used for differential gene expression (DEG) analysis in EdgeR[69]. An FDR (False Discovery
669 Rate) value <0.05 was used as a cut-off of significant differential gene expression. Viral
670 sequences were aligned to the MPXV Clade IIa reference sequence (NC_063383.1). High
671 confidence (FDR <0.05, ≥ 1.5 log2 fold change [FC]) DEGs were used for pathway analysis
672 in Reactome (https://reactome.org)[70,71] or differential pathway analysis in Metascape
673 (https://metascape.org/gp/index.html#/main/step1)[72]. For Reactome analysis, the gene
674 mapping tool was used as a filter to identify pathways enriched (over-represented) for
675 mapped entities. FDR values <0.05 were considered significant for pathway enrichment. In
676 Metascape, all DEGs were used for differential pathway analysis. Pathway *p*-values <0.05
677 were considered significant. Heat maps were plotted in GraphPad Prism (version 10). Mean
678 counts per million (CPM) values of zero were normalized to 0.01 for log2 presentation. Venn
679 diagrams were plotted using http://bioinformatics.psb.ugent.be/webtools/Venn/. RNA-Seq
680 datasets generated from this study have been deposited in the European Nucleotide Archive
681 (ENA), accession number PRJEB66116.
682

683 **Statistical analysis**

684 The number (N) of independent biological experiments is shown throughout. GraphPad
685 Prism (version 10) was used for statistical analysis. Statistical tests and *p*-values are shown
686 throughout. Statistically significant differences were accepted at $p<0.05$.
687

688 **Data availability**

689 All datasets generated and analysed in this study will be made freely available in
690 supplemental files or online (ENA; accession number PRJEB66116) upon manuscript
691 acceptance for publication.

Acknowledgements

The authors would like to thank the members of the MPOX Research Consortium UK for the constructive comments and feedback during the preparation of this manuscript. The authors would also like to thank ISARIC4C for the provision of biological samples used to isolate infectious MPXV. This manuscript is dedicated in memory of Kyriaki Nomikou, an exceptional scientist who sadly passed away during the preparation of this manuscript. Kiki was greatly loved and will be sadly missed by everyone who was blessed to meet her.

Funding:

This work was supported by the Biotechnology and Biological Sciences Research Council (BBSRC) Monkeypox rapid response grant (BB/X011607/1) awarded to ADSF, ET, and CB. CD and ET were funded by the Medical Research Council (MRC; MC_UU_00034/6 awarded to ET). KD was funded by the MRC (MC_UU_00034/2 awarded to Pablo Murcia, University of Glasgow). IE, SMF, and CB were funded by the MRC (MC_UU_12014/5 and MC_UU_00034/2 awarded to CB). JKW was funded by an MRC CVR DTA award (MC_ST_U18018). BB was funded by a Wellcome Trust/Royal Society Sir Henry Dale Fellowship (210462/Z/18/Z). QG, SBV, KN and ADSF were funded by the MRC (MC_UU_00034/6 awarded to ADSF). LO was funded by an MRC precision medicine award (MR/R01566X/1). The funders had no role in study design, data collection and analysis, decision to publish, or preparation of the manuscript.

Competing interests: The authors declare no competing interests exist.

Author Contributions

Data curation: Chris Davis, Ilaria Epifano, Kieran Dee, Steven McFarlane, Quan Gu, Sreenu B. Vattipally, Lily Tong, Kyriaki Nomikou, Lauren Orr, Chris Boutell.

Formal analysis: Chris Davis, Ilaria Epifano, Kieran Dee, Joanna K. Wojtus, Quan Gu, Sreenu B. Vattipally, Chris Boutell.

Funding acquisition: Benjamin Brennan, Ana Da Silva Filipe, Emma Thomson, Chris Boutell.

Investigation: Chris Davis, Ilaria Epifano, Kieran Dee, Lauren Orr, Chris Boutell.

Methodology: Chris Davis, Ilaria Epifano, Steven McFarlane, Benjamin Brennan, Lauren Orr, Chris Boutell.

Project administration: Ana Da Silva Filipe, Antonia Ho, Emma Thomson, Chris Boutell.

Resources: Steven McFarlane, Benjamin Brennan, Ana Da Silva Filipe, Antonia Ho, Emma Thomson, Chris Boutell.

Supervision: Ana Da Silva Filipe, Emma Thomson, Chris Boutell.

Validation: Chris Davis, Ilaria Epifano, Kieran Dee, Chris Boutell.

Visualization: Chris Davis, Ilaria Epifano, Chris Boutell.

Writing – original draft: Chris Davis, Chris Boutell.

Writing – review & editing: Chris Davis, Ilaria Epifano, Chris Boutell.

References

1 Ulaeto, D. *et al.* New nomenclature for mpox (monkeypox) and monkeypox virus clades. *Lancet Infect Dis* **23**, 273-275, doi:10.1016/S1473-3099(23)00055-5 (2023).

2 Nolen, L. D. *et al.* Introduction of Monkeypox into a Community and Household: Risk Factors and Zoonotic Reservoirs in the Democratic Republic of the Congo. *Am J Trop Med Hyg* **93**, 410-415, doi:10.4269/ajtmh.15-0168 (2015).

3 Huang, Y., Mu, L. & Wang, W. Monkeypox: epidemiology, pathogenesis, treatment and prevention. *Signal Transduct Target Ther* **7**, 373, doi:10.1038/s41392-022-01215-4 (2022).

4 El Eid, R., Allaw, F., Haddad, S. F. & Kanj, S. S. Correction: Human monkeypox: A review of the literature. *PLoS Pathog* **18**, e1011008, doi:10.1371/journal.ppat.1011008 (2022).

5 Isidro, J. *et al.* Phylogenomic characterization and signs of microevolution in the 2022 multi-country outbreak of monkeypox virus. *Nat Med* **28**, 1569-1572, doi:10.1038/s41591-022-01907-y (2022).

6 Gigante, C. M. *et al.* Multiple lineages of monkeypox virus detected in the United States, 2021-2022. *Science* **378**, 560-565, doi:10.1126/science.add4153 (2022).

7 O'Toole, Á. *et al.* Putative APOBEC3 deaminase editing in MPXV as evidence for sustained human transmission since at least 2016. *bioRxiv*, 2023.2001.2023.525187, doi:10.1101/2023.01.23.525187 (2023).

8 Thornhill, J. P. *et al.* Monkeypox Virus Infection in Humans across 16 Countries - April-June 2022. *N Engl J Med* **387**, 679-691, doi:10.1056/NEJMoa2207323 (2022).

9 Reynolds, M. G. & Damon, I. K. Outbreaks of human monkeypox after cessation of smallpox vaccination. *Trends Microbiol* **20**, 80-87, doi:10.1016/j.tim.2011.12.001 (2012).

10 Tarin-Vicente, E. J. *et al.* Clinical presentation and virological assessment of confirmed human monkeypox virus cases in Spain: a prospective observational cohort study. *Lancet* **400**, 661-669, doi:10.1016/S0140-6736(22)01436-2 (2022).

11 Fink, D. L. *et al.* Clinical features and management of individuals admitted to hospital with monkeypox and associated complications across the UK: a retrospective cohort study. *Lancet Infect Dis*, doi:10.1016/S1473-3099(22)00806-4 (2022).

12 Palich, R. *et al.* Viral loads in clinical samples of men with monkeypox virus infection: a French case series. *Lancet Infect Dis* **23**, 74-80, doi:10.1016/S1473-3099(22)00586-2 (2023).
13 Mailhe, M. *et al.* Clinical characteristics of ambulatory and hospitalized patients with monkeypox virus infection: an observational cohort study. *Clin Microbiol Infect*, doi:10.1016/j.cmi.2022.08.012 (2022).
14 Jezek, Z., Szczeniowski, M., Paluku, K. M. & Mutombo, M. Human monkeypox: clinical features of 282 patients. *J Infect Dis* **156**, 293-298, doi:10.1093/infdis/156.2.293 (1987).
15 McCollum, A. M. & Damon, I. K. Human monkeypox. *Clin Infect Dis* **58**, 260-267, doi:10.1093/cid/cit703 (2014).
16 Huhn, G. D. *et al.* Clinical characteristics of human monkeypox, and risk factors for severe disease. *Clin Infect Dis* **41**, 1742-1751, doi:10.1086/498115 (2005).
17 Yinka-Ogunleye, A. *et al.* Outbreak of human monkeypox in Nigeria in 2017-18: a clinical and epidemiological report. *Lancet Infect Dis* **19**, 872-879, doi:10.1016/S1473-3099(19)30294-4 (2019).
18 Tofan, V., Lenghel, A., de Camargo, M. M. & Stan, R. C. Fever as an evolutionary agent to select immune complexes interfaces. *Immunogenetics* **74**, 465-474, doi:10.1007/s00251-022-01263-8 (2022).
19 Becskei, A. & Rahaman, S. The life and death of RNA across temperatures. *Comput Struct Biotechnol J* **20**, 4325-4336, doi:10.1016/j.csbj.2022.08.008 (2022).
20 Evans, S. S., Repasky, E. A. & Fisher, D. T. Fever and the thermal regulation of immunity: the immune system feels the heat. *Nat Rev Immunol* **15**, 335-349, doi:10.1038/nri3843 (2015).
21 Ogoina, D. Fever, fever patterns and diseases called 'fever'--a review. *J Infect Public Health* **4**, 108-124, doi:10.1016/j.jiph.2011.05.002 (2011).
22 Alcami, A. & Smith, G. L. A mechanism for the inhibition of fever by a virus. *Proc Natl Acad Sci U S A* **93**, 11029-11034, doi:10.1073/pnas.93.20.11029 (1996).
23 Laloli, L. *et al.* Time-resolved characterization of the innate immune response in the respiratory epithelium of human, porcine, and bovine during influenza virus infection. *Front Immunol* **13**, 970325, doi:10.3389/fimmu.2022.970325 (2022).
24 V'Kovski, P. *et al.* Disparate temperature-dependent virus-host dynamics for SARS-CoV-2 and SARS-CoV in the human respiratory epithelium. *PLoS Biol* **19**, e3001158, doi:10.1371/journal.pbio.3001158 (2021).
25 Dalton, R. M. *et al.* Temperature sensitive influenza A virus genome replication results from low thermal stability of polymerase-cRNA complexes. *Virol J* **3**, 58, doi:10.1186/1743-422X-3-58 (2006).
26 Herder, V. *et al.* Elevated temperature inhibits SARS-CoV-2 replication in respiratory epithelium independently of IFN-mediated innate immune defenses. *PLoS Biol* **19**, e3001065, doi:10.1371/journal.pbio.3001065 (2021).
27 Earn, D. J., Andrews, P. W. & Bolker, B. M. Population-level effects of suppressing fever. *Proc Biol Sci* **281**, 20132570, doi:10.1098/rspb.2013.2570 (2014).
28 Ryan, M. & Levy, M. M. Clinical review: fever in intensive care unit patients. *Crit Care* **7**, 221-225, doi:10.1186/cc1879 (2003).
29 Schulman, C. I. *et al.* The effect of antipyretic therapy upon outcomes in critically ill patients: a randomized, prospective study. *Surg Infect (Larchmt)* **6**, 369-375, doi:10.1089/sur.2005.6.369 (2005).
30 Hutson, C. L. *et al.* A prairie dog animal model of systemic orthopoxvirus disease using West African and Congo Basin strains of monkeypox virus. *J Gen Virol* **90**, 323-333, doi:10.1099/vir.0.005108-0 (2009).

31 Hutson, C. L. *et al.* Laboratory Investigations of African Pouched Rats (Cricetomys gambianus) as a Potential Reservoir Host Species for Monkeypox Virus. *PLoS Negl Trop Dis* **9**, e0004013, doi:10.1371/journal.pntd.0004013 (2015).
32 Tree, J. A. *et al.* Sequence of pathogenic events in cynomolgus macaques infected with aerosolized monkeypox virus. *J Virol* **89**, 4335-4344, doi:10.1128/JVI.03029-14 (2015).
33 Bedson, H. S. & Dumbell, K. R. The effect of temperature on the growth of pox viruses in the chick embryo. *J Hyg (Lond)* **59**, 457-469, doi:10.1017/s0022172400039152 (1961).
34 Dumbell, K. R. & Bedson, H. S. The Use of Ceiling Temperature and Reactivation in the Isolation of Pox Virus Hybrids. *J Hyg (Lond)* **62**, 133-140, doi:10.1017/s0022172400039863 (1964).
35 Molteni, C., Forni, D., Cagliani, R., Clerici, M. & Sironi, M. Genetic ancestry and population structure of vaccinia virus. *NPJ Vaccines* **7**, 92, doi:10.1038/s41541-022-00519-4 (2022).
36 Senkevich, T. G., Yutin, N., Wolf, Y. I., Koonin, E. V. & Moss, B. Ancient Gene Capture and Recent Gene Loss Shape the Evolution of Orthopoxvirus-Host Interaction Genes. *mBio* **12**, e0149521, doi:10.1128/mBio.01495-21 (2021).
37 Qin, L., Liang, M. & Evans, D. H. Genomic analysis of vaccinia virus strain TianTan provides new insights into the evolution and evolutionary relationships between Orthopoxviruses. *Virology* **442**, 59-66, doi:10.1016/j.virol.2013.03.025 (2013).
38 Thompson, R. L. & Coates, M. S. The Effect of Temperature upon the Growth and Survival of Myxoma, Herpes, and Vaccinia Viruses in Tissue Culture. *The Journal of Infectious Diseases* **71**, 83-85, doi:10.1093/infdis/71.1.83 (1942).
39 Forni, D., Cagliani, R., Pozzoli, U. & Sironi, M. An APOBEC3 Mutational Signature in the Genomes of Human-Infecting Orthopoxviruses. *mSphere* **8**, e0006223, doi:10.1128/msphere.00062-23 (2023).
40 Suspene, R. *et al.* APOBEC3F is a mutational driver of the human Monkeypox virus identified in the 2022 outbreak. *J Infect Dis*, doi:10.1093/infdis/jiad165 (2023).
41 Moein, S., Javanmard, S. H., Abedi, M., Izadpanahi, M. H. & Gheisari, Y. Identification of Appropriate Housekeeping Genes for Gene Expression Analysis in Long-term Hypoxia-treated Kidney Cells. *Adv Biomed Res* **6**, 15, doi:10.4103/2277-9175.200790 (2017).
42 Curina, A. *et al.* High constitutive activity of a broad panel of housekeeping and tissue-specific cis-regulatory elements depends on a subset of ETS proteins. *Genes Dev* **31**, 399-412, doi:10.1101/gad.293134.116 (2017).
43 Eisenberg, E. & Levanon, E. Y. Human housekeeping genes, revisited. *Trends Genet* **29**, 569-574, doi:10.1016/j.tig.2013.05.010 (2013).
44 Lum, F. M. *et al.* Monkeypox: disease epidemiology, host immunity and clinical interventions. *Nat Rev Immunol* **22**, 597-613, doi:10.1038/s41577-022-00775-4 (2022).
45 Li, H. *et al.* The land-scape of immune response to monkeypox virus. *EBioMedicine* **87**, 104424, doi:10.1016/j.ebiom.2022.104424 (2023).
46 Johnston, S. C. *et al.* Cytokine modulation correlates with severity of monkeypox disease in humans. *J Clin Virol* **63**, 42-45, doi:10.1016/j.jcv.2014.12.001 (2015).
47 Joklik, W. K., Abel, P. & Holmes, I. H. Reactivation of poxviruses by a non-genetic mechanism. *Nature* **186**, 992-993, doi:10.1038/186992b0 (1960).
48 Sood, C. L. & Moss, B. Vaccinia virus A43R gene encodes an orthopoxvirus-specific late non-virion type-1 membrane protein that is dispensable for replication but

865 enhances intradermal lesion formation. *Virology* **396**, 160-168,
866 doi:10.1016/j.virol.2009.10.025 (2010).
867 49 Tanaka-Kataoka, M. *et al.* In vivo antiviral effect of interleukin 18 in a mouse model
868 of vaccinia virus infection. *Cytokine* **11**, 593-599, doi:10.1006/cyto.1998.0453 (1999).
869 50 Symons, J. A. *et al.* The vaccinia virus C12L protein inhibits mouse IL-18 and
870 promotes virus virulence in the murine intranasal model. *J Gen Virol* **83**, 2833-2844,
871 doi:10.1099/0022-1317-83-11-2833 (2002).
872 51 Clark, R. H., Kenyon, J. C., Bartlett, N. W., Tscharke, D. C. & Smith, G. L. Deletion
873 of gene A41L enhances vaccinia virus immunogenicity and vaccine efficacy. *J Gen*
874 *Virol* **87**, 29-38, doi:10.1099/vir.0.81417-0 (2006).
875 52 El-Radhi, A. S. in *Clinical Manual of Fever in Children* (ed A. Sahib El-Radhi) 53-
876 68 (Springer International Publishing, 2018).
877 53 Johnston, S. C. *et al.* In vitro inhibition of monkeypox virus production and spread by
878 Interferon-beta. *Virol J* **9**, 5, doi:10.1186/1743-422X-9-5 (2012).
879 54 Stabenow, J. *et al.* A mouse model of lethal infection for evaluating prophylactics and
880 therapeutics against Monkeypox virus. *J Virol* **84**, 3909-3920,
881 doi:10.1128/JVI.02012-09 (2010).
882 55 Arndt, W. D. *et al.* Evasion of the Innate Immune Type I Interferon System by
883 Monkeypox Virus. *J Virol* **89**, 10489-10499, doi:10.1128/JVI.00304-15 (2015).
884 56 Hernaez, B. *et al.* A virus-encoded type I interferon decoy receptor enables evasion of
885 host immunity through cell-surface binding. *Nat Commun* **9**, 5440,
886 doi:10.1038/s41467-018-07772-z (2018).
887 57 Arndt, W. D. *et al.* Monkeypox virus induces the synthesis of less dsRNA than
888 vaccinia virus, and is more resistant to the anti-poxvirus drug, IBT, than vaccinia
889 virus. *Virology* **497**, 125-135, doi:10.1016/j.virol.2016.07.016 (2016).
890 58 Conn, K. L. *et al.* Novel Role for Protein Inhibitor of Activated STAT 4 (PIAS4) in
891 the Restriction of Herpes Simplex Virus 1 by the Cellular Intrinsic Antiviral Immune
892 Response. *J Virol* **90**, 4807-4826, doi:10.1128/JVI.03055-15 (2016).
893 59 Piboonniyom, S. O. *et al.* Abrogation of the retinoblastoma tumor suppressor
894 checkpoint during keratinocyte immortalization is not sufficient for induction of
895 centrosome-mediated genomic instability. *Cancer Res* **63**, 476-483 (2003).
896 60 Meyers, C. Organotypic (raft) epithelial tissue culture system for the differentiation-
897 dependent replication of papillomavirus. *Methods in Cell Science* **18**, 201-210,
898 doi:10.1007/BF00132885 (1996).
899 61 Carter, G. C. *et al.* Vaccinia virus cores are transported on microtubules. *J Gen Virol*
900 **84**, 2443-2458, doi:10.1099/vir.0.19271-0 (2003).
901 62 Kotwal, G. J. & Abrahams, M.-R. in *Vaccinia Virus and Poxvirology: Methods and*
902 *Protocols* (ed Stuart N. Isaacs) 101-112 (Humana Press, 2004).
903 63 Everett, R. D., Boutell, C. & Orr, A. Phenotype of a herpes simplex virus type 1
904 mutant that fails to express immediate-early regulatory protein ICP0. *J Virol* **78**,
905 1763-1774, doi:10.1128/jvi.78.4.1763-1774.2004 (2004).
906 64 Katoh, K., Misawa, K., Kuma, K. & Miyata, T. MAFFT: a novel method for rapid
907 multiple sequence alignment based on fast Fourier transform. *Nucleic Acids Res* **30**,
908 3059-3066, doi:10.1093/nar/gkf436 (2002).
909 65 Baker, J. L. & Ward, B. M. Development and comparison of a quantitative TaqMan-
910 MGB real-time PCR assay to three other methods of quantifying vaccinia virions. *J*
911 *Virol Methods* **196**, 126-132, doi:10.1016/j.jviromet.2013.10.026 (2014).
912 66 Davi, S. D. *et al.* Recombinase polymerase amplification assay for rapid detection of
913 Monkeypox virus. *Diagn Microbiol Infect Dis* **95**, 41-45,
914 doi:10.1016/j.diagmicrobio.2019.03.015 (2019).

915 67 Kim, D., Langmead, B. & Salzberg, S. L. HISAT: a fast spliced aligner with low
916 memory requirements. *Nat Methods* **12**, 357-360, doi:10.1038/nmeth.3317 (2015).
917 68 Liao, Y., Smyth, G. K. & Shi, W. featureCounts: an efficient general purpose program
918 for assigning sequence reads to genomic features. *Bioinformatics* **30**, 923-930,
919 doi:10.1093/bioinformatics/btt656 (2014).
920 69 Robinson, M. D., McCarthy, D. J. & Smyth, G. K. edgeR: a Bioconductor package
921 for differential expression analysis of digital gene expression data. *Bioinformatics* **26**,
922 139-140, doi:10.1093/bioinformatics/btp616 (2010).
923 70 Fabregat, A. *et al.* The Reactome Pathway Knowledgebase. *Nucleic Acids Res* **46**,
924 D649-D655, doi:10.1093/nar/gkx1132 (2018).
925 71 Jassal, B. *et al.* The reactome pathway knowledgebase. *Nucleic Acids Res* **48**, D498-
926 D503, doi:10.1093/nar/gkz1031 (2020).
927 72 Zhou, Y. *et al.* Metascape provides a biologist-oriented resource for the analysis of
928 systems-level datasets. *Nat Commun* **10**, 1523, doi:10.1038/s41467-019-09234-6
929 (2019).
930 73 Shaw, A. E. *et al.* Fundamental properties of the mammalian innate immune system
931 revealed by multispecies comparison of type I interferon responses. *PLoS Biol* **15**,
932 e2004086, doi:10.1371/journal.pbio.2004086 (2017).
933
934
935
936

937 ## Figure Legends

938 **Fig 1. Clinical MPXV isolation and genotyping.** Skin swabs obtained from a hospitalised
939 MPXV PCR positive patient presenting with fever and rash during the 2022 mpox outbreak
940 were used to isolate and amplify infectious virus. Clinical swabs (CVR_MPXV1a) and
941 supernatant derived from primary amplification (MPXV CVR_S1) were subjected to
942 Illumina sequencing and confirmed to be identical (accession number ON808413). (A)
943 Phylogenetic tree highlighting the evolutionary and taxonomic relationship of MPXV
944 CVR_S1 (red text) to other sequenced MPXV Clade IIa and IIb strains (as indicated). (B)
945 Schematic diagram highlighting the position and distribution of the 67 single nucleotide
946 polymorphisms (SNPs; S1 data) identified within the MPXV CVR_S1 genome relative to the
947 MPXV Clade IIa reference strain (NC_063383-A; blue text). Blue lines (guanine to adenine,
948 G to A), red lines (cytosine to thymine, C to T), yellow lines (adenine to guanine, A to G),
949 green lines (thymine to cytosine, T to C).
950

951 **Fig 2. Tissue temperature influences the outcome of MPXV replication in skin**
952 **epithelium.** Human keratinocytes were differentiated into pseudostratified skin epithelium
953 under ALI for 12 to 14 days. Tissues were mock treated or MPXV infected (MOI 10^2 or 10^3

954 PFU/tissue) for 1 h at 37 °C prior to incubation at 33, 37, or 40 °C for 72 h (as indicated). (A)
955 Representative immunohistochemistry (IHC) stained tissue sections counter-stained with
956 haematoxylin. Brown highlights epithelial regions positive for MPXV virion antigen
957 expression. Scale bar 0.25 mm. (B) Quantitation of epithelial thickness of mock treated or
958 MPXV infected tissues (as in A). Mean and 95% CI shown. Values derived from a minimum
959 of 40 measurements per tissue; *p*-values shown, Kruskal-Wallis one-way ANOVA. (C)
960 Quantitation of MPXV infected tissue area. Values normalised to infected tissues incubated
961 at 37 °C. Mean and SD shown. (D) Proportion of weak, moderate, and strong MPXV virion
962 antigen positive cells. Values normalised to the proportion of strong MPXV antigen-stained
963 cells from infected tissues incubated at 37 °C per biological experiment. (C/D) *P*-values
964 shown, one sample two-tailed t test against a theoretical mean of 1. (A to D) *N*=3
965 independent biological experiments. Raw values presented in S2 data. Original tissue section
966 scans are shown in Fig S1.
967
968 **Fig 3. Temperature elevation inhibits MPXV replication.** Human foreskin fibroblast (HFt)
969 cells were infected with VACV (MOI 0.0005 or 0.1 PFU/cell, A to D or E, respectively; top
970 panels) or MPXV (MOI 0.001 or 0.1 PFU/cell, F to I or J, respectively; bottom panels) for 1
971 h at 37 °C prior to incubation at 33, 37, 38.5 or 40 °C. (A/F) Representative images of VACV
972 or MPXV infected cell monolayers stained with Coomassie Brilliant blue at 48 h post-
973 infection (hpi). (B/G) Quantitation of VACV or MPXV plaque counts at 48 hpi. Means and
974 SD shown; *p*-values shown, Dunnett's unpaired one-way ANOVA. (C/H) Quantitation of
975 plaque diameters at 48 hpi. Values normalised to the geometric mean at 33 °C per biological
976 experiment. Means and 95% CI shown; *p*-values shown, Kruskai-Wallis one-way ANOVA.
977 (D/I) Quantitation (log10 PFU/ml) of cell-released virus from infected HFt cells quantified
978 by plaque assay in Vero E6 cells. Mean and SD shown; *p*-values shown, Dunnett's unpaired
979 one-way ANOVA. Limit of detection (LOD) shown (dotted grey line). (E/F) qPCR
980 quantitation of virus host-cell entry at 1 hpi. Values normalised to 37 °C per biological
981 experiment. All data points shown; line, mean; whisker, SD; *p*-values shown, one sample
982 two-tailed t test against a theoretical mean of 1. (A to J) *N*≥3 independent biological
983 experiments. Raw values presented in S3 data.
984
985 **Fig 4. Basal host-cell temperature influences MPXV replication in a cell-type dependent**
986 **manner.** Confluent HFt, NOK (human normal oral keratinocyte), RPE (human retinal
987 pigmented epithelial), Vero E6 (green monkey kidney epithelial), or CV-1 (green monkey

988 kidney fibroblast) cell monolayers were infected with VACV (MOI 0.0005 PFU/cell; top
989 panels) or MPXV (MOI 0.001 PFU/cell; bottom panels) for 1 h at 37 °C prior to incubation at
990 33, 37, 38.5 or 40 °C. Infected cell monolayers were stained with Coomassie Brilliant blue at
991 48 h post-infection and plaque counts quantified. Values were normalised to 37 °C per cell
992 line per biological experiment (grey dotted line). (A/C) Normalised plaque counts per cell
993 line over the temperature range of analysis. Means and SD shown; *p*-values shown, one
994 sample two-tailed t test against a theoretical mean of 1. (B/D) Normalised plaque counts per
995 temperature condition. Means and SD shown; *p*-values shown, Dunnett's unpaired one-way
996 ANOVA. (A to D) *N*=3 independent biological experiments. Raw values presented in S4
997 data.
998
999 **Fig 5. Basal host-cell temperature differentially influences the regulation of MPXV**
1000 **transcription.** HFt cells were infected with MPXV (MOI 0.01 PFU/cell) for 1 h at 37 °C
1001 prior to incubation at 33, 37, 38.5 or 40 °C. RNA was extracted at 48 h post-infection (hpi)
1002 for RNA-Seq. Viral reads were aligned to the MPXV reference sequence (NC_063383.1).
1003 Mapped read (MR) counts were used to quantify MPXV gene expression levels. (A)
1004 Principal Component (PC) analysis of MPXV MR counts. (B) Line graph showing MR count
1005 per ORF (log10). Purple circles and text highlight viral ORFs < 10 MR (dotted line). (C)
1006 Expression level of MPXV ORFs (log2 MR); every third ORF labelled. (D) Expression level
1007 of MPXV ORFs relating to the viral RNA (vRNA) polymerase complex, viral toll like
1008 receptor (vTLR) antagonists, and intracellular mature virus (IMV) assembly (as indicated).
1009 Purple text highlights viral ORFs < 10 MR (as in B). (E) Line graph showing normalised MR
1010 count per ORF (log2 MR) at 33 and 38.5 °C. Values were normalised to MR counts at 37 °C
1011 (solid grey line). Orange circles and text highlight viral ORFs ≥ 1.5 log2 FC (fold change)
1012 relative to 37 °C (dotted grey line). (A to E) *N*=3 independent biological experiments; *p*-
1013 values shown, Dunnett's paired one-way ANOVA (bottom), paired two-tailed *t* test (top).
1014 Raw values presented in S5 data.
1015
1016 **Fig 6. Basal temperature influences the host-cell response to MPXV infection.** HFt cells
1017 were mock treated or infected with MPXV (MOI 0.01 PFU/cell) for 1 h at 37 °C prior to
1018 incubation at 33, 37, 38.5 or 40 °C. RNA was extracted at 48 h post-infection (hpi) for RNA-
1019 Seq. Host mapped reads were aligned to the human genome, normalised to counts per million
1020 (CPM), and DEGs (FDR < 0.05, ≥ 1.5 log2 FC) identified for each paired condition analysed
1021 (as indicated). (A) Venn diagram showing the number of unique or shared DEGs between

1022 each paired condition. (B) Circos plots showing the proportion of unique (light orange inner
1023 circle) or shared (dark orange inner circle + purple lines) DEGs between each paired
1024 condition. (C) Metascape pathway analysis showing significant up-regulated DEG
1025 enrichment (*p*-value < 0.05; log10 *p*-values shown) for each paired condition (as in A/B).
1026 Black arrows highlight enriched for cytokine related pathways; grey boxes, *p*-value > 0.05.
1027 (D) Expression level (log2 CPM) of cytokine related DEGs identified to be upregulated in
1028 response to MPXV infection (black arrows in C, 71 genes in total; log2 CPM). (E) Principal
1029 Component (PC) analysis of cytokine related DEGs (as in D) in mock treated and MPXV
1030 infected cells (as indicated). Purple arrow highlights MPXV 40 °C expression levels
1031 clustering with mock treated samples. (F) Expression profile of cytokine related DEGs (as in
1032 D). Black line, median; whisker, 95% CI; all data points shown. (G) Expression level (log2
1033 CPM) of host interferon (IFN)-related receptors and cytokines in mock treated or MPXV
1034 infected cells. Black arrow highlights expression level of *IFNB1* in mock treated or MPXV
1035 infected cells. (D, F, G) *P*-values shown, Dunnett's paired one-way ANOVA. (A to G) *N*=3
1036 independent biological experiments. Raw values presented in S6 data.
1037
1038 **Fig 7. Basal host-cell temperature influences the interleukin response to MPXV**
1039 **infection.** HFt cells were mock treated or infected with MPXV (MOI 0.01 PFU/cell) for 1 h
1040 at 37 °C prior to incubation at 33, 37, 38.5 or 40 °C. RNA was extracted at 48 h post-
1041 infection (hpi) for RNA-Seq. Host mapped reads were aligned to the human genome,
1042 normalised to counts per million (CPM), and DEGs (FDR < 0.05, ≥ 1.5 log2 FC) identified.
1043 (A) Scatter plot showing DEGs identified between MPXV infected cells incubated at 37 and
1044 40 °C; up-regulated, red circles; down-regulated, blue circles. (B) Reactome pathway
1045 analysis of down-regulated mapped DEGs (blue circles in A). Top 25 down-regulated
1046 pathways (FDR < 0.05) shown (blue bars; plotted as -log10 FDR). Dotted line, threshold of
1047 significance (-log10 FDR of 0.05). Pathways relating to cell cycle (grey arrow and circle) and
1048 immune system regulation (coloured arrows and circles) are highlighted. (C) Venn diagram
1049 showing the number of unique or shared DEGs identified in immune system pathways
1050 (coloured arrows and circles identified in B). (D) Expression level (log2 CPM) of immune
1051 system DEGs (identified in B; 61 genes in total); *p*-values shown, Dunnett's unpaired one-
1052 way ANOVA (top), unpaired two-tailed *t* test (bottom). DEGs associated with Signalling by
1053 Interleukins (ILs) highlighted (green circles). (E) Expression profile (CPM) of selected
1054 interleukins (IL6, IL11, and IL12A) and chemokines (CXCL1, CXCL6, CXCL2, CXCL3) in

1055 mock treated (grey lines) and MPXV infected (green lines) cells across the temperature range
1056 of analysis; *p*-values shown, unpaired two-tailed *t* test. Raw values presented in S7 Data.
1057
1058 **Fig 8. Temperature elevation enhances the type-I IFN-mediated host-cell restriction of**
1059 **MPXV.** (A to D) HFt cells were pre-treated with IFN-β (0 to 100 IU/ml, as indicated) for 16
1060 h at 33, 37, 38.5 or 40 °C prior to MPXV (MOI 0.001 PFU/cell) infection (1 h at 37 °C) and
1061 continued incubation at their respective incubation temperatures in the presence of IFN. (A)
1062 Representative images of MPXV infected cell monolayers pre-treated with IFN and stained
1063 with Coomassie Brilliant blue at 48 h post-infection (hpi). (B) Quantitation of MPXV plaque
1064 counts at 48 hpi (as shown in A). Means and SD shown. Grey dotted lines and circles
1065 highlight absence of plaque formation at 40 °C. (C/D) Relative MPXV plaque counts. Values
1066 were normalised to no IFN treatment (dotted grey line) per incubation temperature. (C)
1067 Means and SD shown; coloured lines and text, linear regression and corresponding R^2 values.
1068 (D) As in C, all data points shown; black line, mean; whisker, SD; *p*-values shown, Dunnett's
1069 unpaired one-way ANOVA. (E to J) Naïve HFt cells were infected with MPXV (MOI 0.01
1070 PFU/cell) for 1 h at 37 °C prior to overlay with media containing IFN-β (0 to 200 IU/ml, as
1071 indicated) and incubation at 33, 37, 38.5 or 40 °C. (E/F) Cells were fixed at 24 h and stained
1072 for MPXV virion protein expression and the number of antigen positive cells quantified by
1073 indirect immunofluorescence. (E) Mean MPXV positive cell counts (x100) per infected cell
1074 monolayer. (F) As in E, mean and SD shown. (G to J) Infected or infected and IFN treated
1075 monolayers incubated at 37 or 40 °C were either fixed at 48 h or washed and overlayed with
1076 fresh media (IFN washout) and incubation at 37 °C for an additional 48 h prior to fixation at
1077 Coomassie Brilliant blue staining. (G) Quantitation of MPXV plaque counts in cell
1078 monolayers incubated at 40 °C or temperature downshifted from 40 to 37 °C (40>37) with
1079 continued incubation. (H) Quantitation of MPXV plaque counts in cell monolayers incubated
1080 at 37 °C in the presence of IFN or following IFN washout and continued incubation. All data
1081 points shown. (J) Quantitation of MPXV plaque counts in cell monolayers incubated at 37 or
1082 40 °C in the presence of IFN (1 to 200 IU/ml, as indicated) with IFN washout at 48 h and
1083 continued incubation at 37 °C (no IFN). All data points shown. (G to J) Values were
1084 normalised to plaque counts determined at 37 °C (no IFN treatment at 48 h). Mean and SD
1085 shown; *p*-values shown, unpaired two-tailed *t* test. Raw values presented in S8 Data.
1086

1087 **Fig S1. Tissue temperature influences the outcome of MPXV replication in skin**
1088 **epithelium.** Human keratinocytes were seed onto fibroblast-containing collagen coated 6.5
1089 mm transwells and differentiated under ALI for 14 days. Pseudostratified skin epithelium
1090 cultures were mock treated (media only) or MPXV infected (MOI 10^2 or 10^3 PFU/tissue) for
1091 1 h at 37 °C prior to incubation at 33, 37, or 40 °C (as indicated) for 72 h. Whole tissue
1092 sections were stained for MPXV virion antigen expression by immunohistochemistry and
1093 counter stained with eosin. Scale bar = 0.5 mm.
1094
1095 **Fig S2. Temperature elevation inhibits OPXV replication.** (A) Quantitation of DAPI
1096 stained nuclei in mock treated HFt cells incubated at 33, 37, 38.5 or 40 °C for 48 h. (B) MTS
1097 cell viability assay of mock treated or puromycin (Puro, 1 µg/ml; positive control) treated
1098 HFt cells incubated at 37 or 40 °C for 24 h (as indicated). (C to E) Confluent HFt (human
1099 foreskin fibroblast), NOK (human normal oral keratinocyte), RPE (human retinal pigmented
1100 epithelial), Vero E6 (green monkey kidney epithelial), or CV-1 (green monkey kidney
1101 fibroblast) cell monolayers were infected with (C) HSV-1 (MOI 0.002 PFU/cell), (D) VACV
1102 (MOI 0.0005 PFU/cell), or (E) MPXV (MOI 0.001 PFU/cell) for 1 h at 37 °C prior to overlay
1103 and incubation at 33, 37, 38.5 or 40 °C. Infected cell monolayers were fixed at 48 h and
1104 stained with Coomassie Brilliant blue. (C) Quantitation of HSV-1 plaque counts in HFt cells
1105 over the temperature incubation range of analysis. Values were normalised to plaque counts
1106 at 37 °C. Means and SD shown; *p*-values shown, one sample two-tailed t test against a
1107 theoretical mean of 1. (D/E) Representative images of VACV or MPXV infected HFT, RPE,
1108 NOK, Vero E6 (Meso), and CV-1 cell monolayers stained with Coomassie Brilliant blue at
1109 48 h post-infection (hpi). (A to E) $N \geq 3$ independent biological experiments. Raw values
1110 presented in S9 data.
1111
1112 **Fig S3. Basal host-cell temperature differentially influences the regulation of MPXV**
1113 **transcription.** HFt cells were infected with MPXV (MOI 0.01 PFU/cell) for 1 h at 37 °C
1114 prior to incubation at 33, 37, 38.5 or 40 °C. RNA was extracted at 48 h post-infection (hpi)
1115 for RNA-Seq. Host sequences were aligned to the human genome and mapped read (MR)
1116 counts normalised to counts per million (CPM). Viral sequences were aligned to the MPXV
1117 reference sequence (NC_063383.1) and viral MR counts used to quantify MPXV gene
1118 expression levels. (A) Expression level (log2 CPM) of 28 host reference genes over the
1119 temperature range of analysis. (B) Host MR counts in mock treated (grey bars) and MPXV

1120 infected (green bars) cells over the temperature range of analysis. (C) Viral MR counts in
1121 MPXV infected cells over the temperature range of analysis. (D) Expression profile (log2
1122 MR) of seven MPXV ORFs identified at 40 °C ≤ 10 MR counts. (E) Expression profile (log2
1123 MR) of five MPXV ORFs at 33 °C ≥ 1.5 log2 fold-change (FC) downregulated MR count
1124 relative to incubation at 37 °C. (A to E) *N*=3 independent biological experiments; *p*-values
1125 shown, unpaired Dunnett's one-way ANOVA. Raw values presented in S10 data.
1126
1127 **Fig S4. MPXV infection does not stimulate the induction of the type-I IFN response.** HFt
1128 cells were mock treated or infected with MPXV (MOI 0.01 PFU/cell) for 1 h at 37 °C prior to
1129 incubation at 33, 37, 38.5 or 40 °C. RNA was extracted at 48 h post-infection (hpi) for RNA-
1130 Seq. Host sequences were aligned to the human genome and mapped read (MR) counts
1131 normalised to counts per million (CPM). (A) Expression level (log2 CPM) of host interferon
1132 (IFN)-related receptors and cytokines in mock treated or MPXV infected cells over the
1133 temperature range of analysis. (B) Expression profile (CPM) of IFNB1 (circles) and IL-6
1134 (squares) transcript levels in mock treated (grey lines) or MPXV infected (pink lines) cells
1135 over the temperature range of analysis. Means and SD shown. (C/D) Expression profile (log2
1136 CPM) of 489 interferon responsive genes previously identified to be upregulated in response
1137 to universal interferon[73]; every 8th gene labelled. Grey lines in C highlight profile similarity
1138 between experimental conditions. (E) Expression profile (log2 CPM) of host genes associated
1139 with Cytokine Signalling in Immune System (R-HAS-1280215; 715 genes in total) in mock
1140 treated or MPXV infected cells over the temperature range of analysis. (F) Expression profile
1141 (log2 CPM) of host genes associated with Signalling by Interleukins (R-HAS-449147; 459
1142 genes in total) in mock treated or MPXV infected cells over the temperature range of
1143 analysis. (A to G) *N*=3 independent biological experiments. Raw values presented in S11
1144 data. (D to F) *P*-values shown, Dunnett's paired one-way ANOVA with Giesser-Greenhouse
1145 correction.
1146
1147 **Fig S5. Temperature elevation enhances the type-I IFN-mediated host-cell restriction of**
1148 **VACV.** (A to D) HFt cells were pre-treated with IFN-β (0 to 100 IU/ml, as indicated) for 16
1149 h at 33, 37, 38.5 or 40 °C prior to VACV (MOI 0.0005 PFU/cell) infection (1 h at 37 °C) and
1150 continued incubation at their respective temperatures in the presence of IFN. (A)
1151 Representative images of VACV infected cell monolayers pre-treated with IFN and stained
1152 with Coomassie Brilliant blue at 48 h post-infection (hpi). (B) Quantitation of VACV plaque

1153 counts at 48 hpi (as shown in A). Means and SD shown. (C/D) Relative VACV plaque
1154 counts). Values were normalised to no IFN treatment (dotted grey line) per incubation
1155 temperature. (C) Means and SD shown; coloured lines and text, linear regression and
1156 corresponding R^2 values. (D) As in C, all data points shown; black line, mean; whisker, SD;
1157 *p*-values shown, Dunnett's unpaired one-way ANOVA. (E to J) Naïve HFt cells were
1158 infected with VACV (MOI 0.01 PFU/cell, E and F; MOI 0.0005 PFU/cell, G to J) for 1 h at
1159 37 °C prior to overlay with media containing IFN-β (0 to 200 IU/ml, as indicated) and
1160 incubation at 33, 37, 38.5 or 40 °C. (E/F) Cells were fixed at 24 h and stained for VACV
1161 virion protein expression and the number of antigen positive cells quantified by indirect
1162 immunofluorescence. (E) Mean VACV positive cell counts (x1000) per infected cell
1163 monolayer. (F) As in E, mean and SD shown. (G to J) Infected or infected and IFN treated
1164 monolayers incubated at 37 or 40 °C were either fixed at 24 h or washed and overlayed with
1165 fresh media (IFN washout) and incubation at 37 °C for an additional 24 h prior to fixation
1166 and staining. (G) Quantitation of VACV plaque counts in cell monolayers incubated at 40 °C
1167 or temperature downshifted from 40 to 37 °C (40>37) with continued incubation for 24 h. (H)
1168 Quantitation of VACV plaque counts in cell monolayers incubated at 37 or 40 °C in the
1169 presence of IFN (red and blues circles plus solid lines, respectively) or following IFN
1170 washout and continued incubation at 37 °C for 24 h (red and blue squares plus dotted lines,
1171 respectively). (J) Values presented for IFN washout and continued incubation at 37 °C for 24
1172 (red and blue squares in H), all data points shown. (G to J) Values were normalised to plaque
1173 counts determined at 37 °C (no IFN treatment at 24 h). Mean and SD shown; *p*-values shown,
1174 unpaired two-tailed *t* test. Raw values presented in S12 Data.
1175

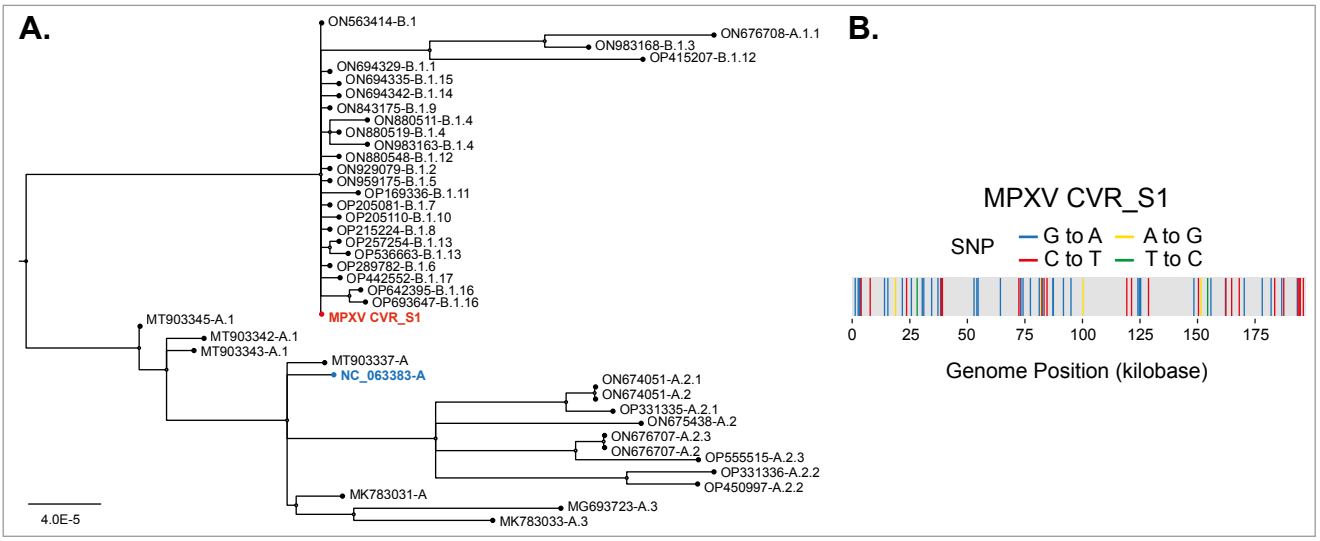

Figure 1. Clinical MPOX virus isolation and genotyping.

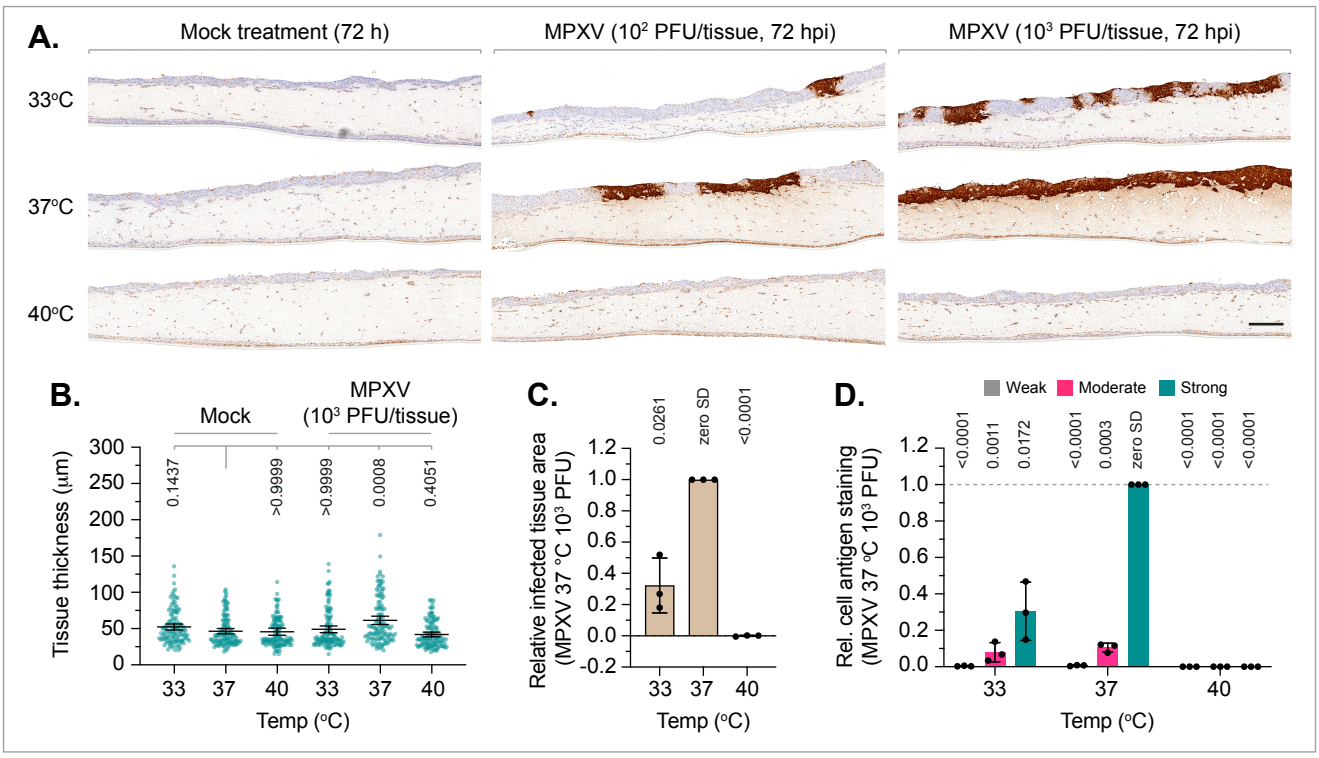

Figure 2. Tissue temperature influences the outcome of MPXV infection in skin epithelium

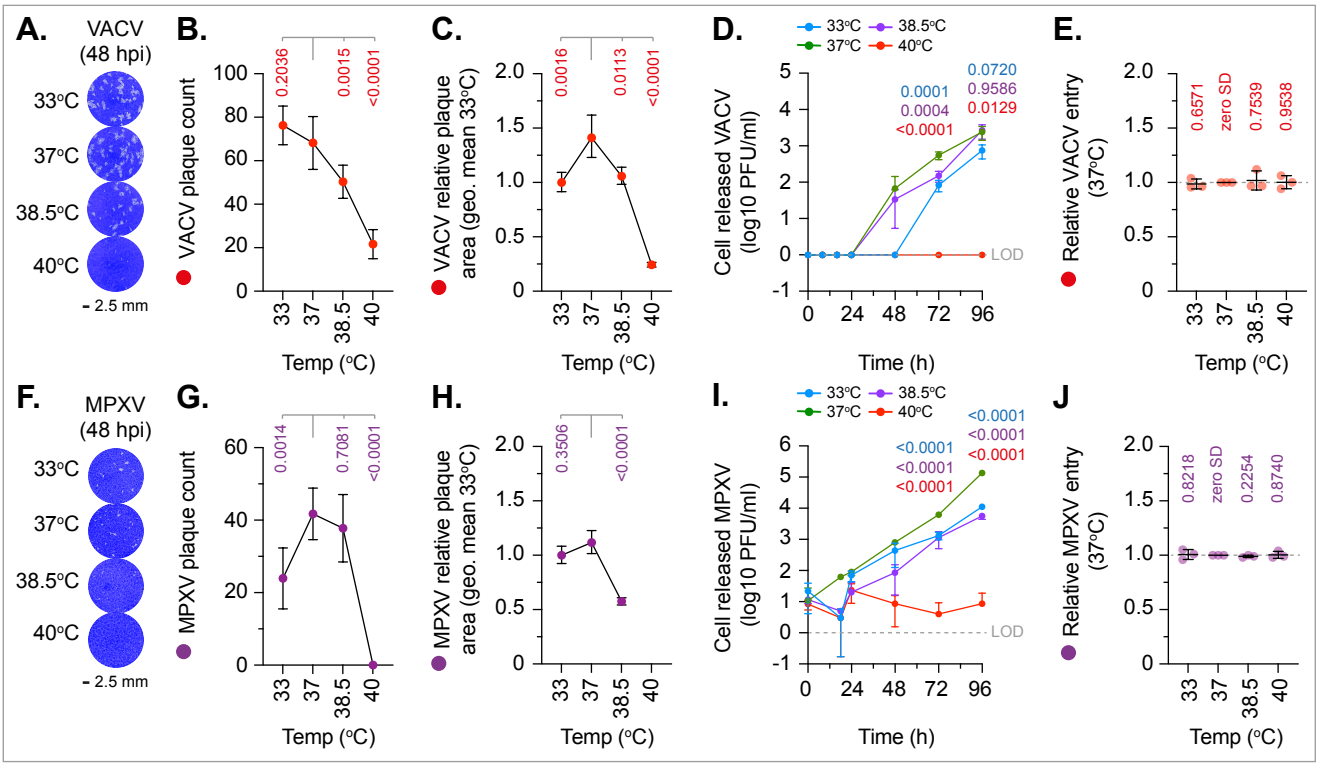

Figure 3. Temperature elevation inhibits MPXV replication

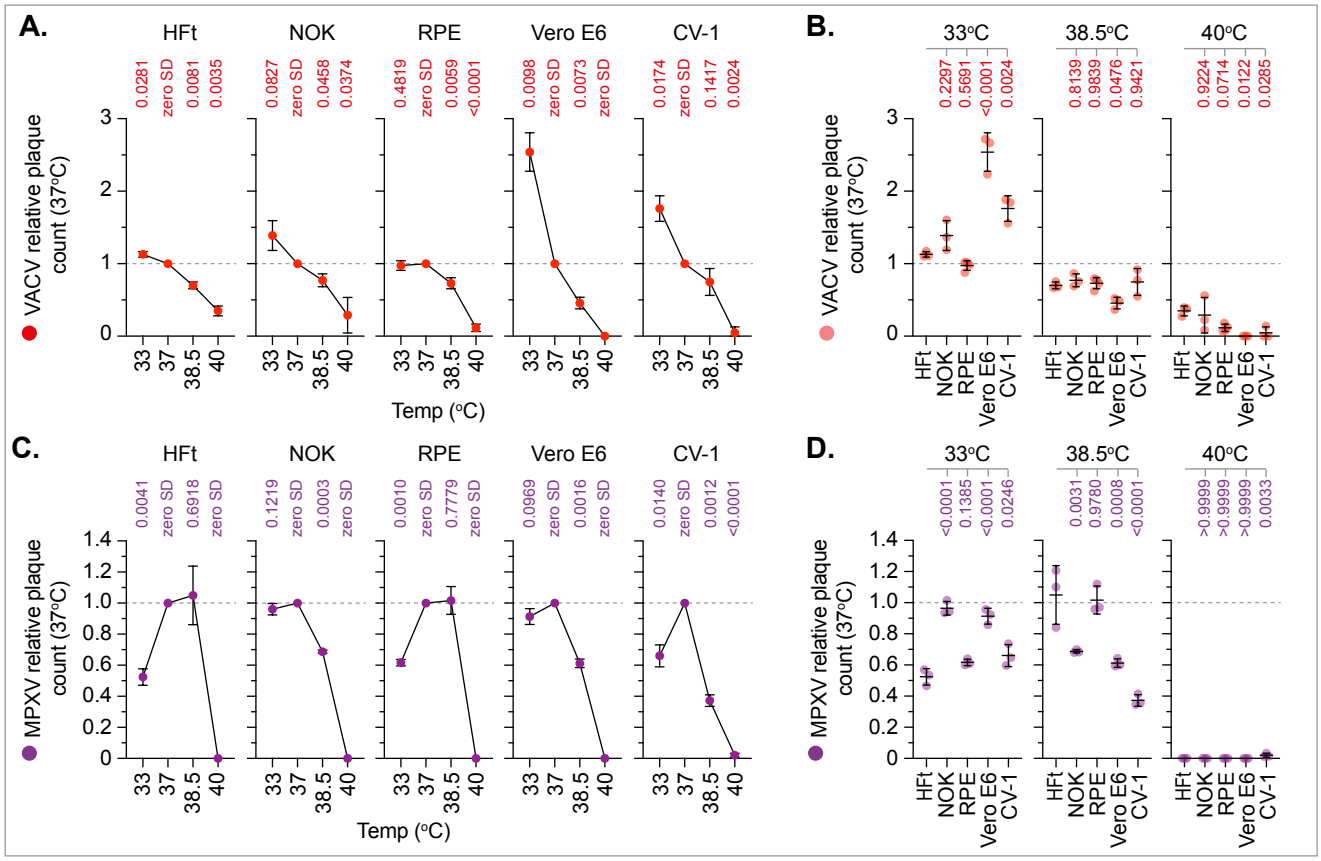

Figure 4. Basal host-cell temperature influences MPXV replication in a cell-type dependent manner

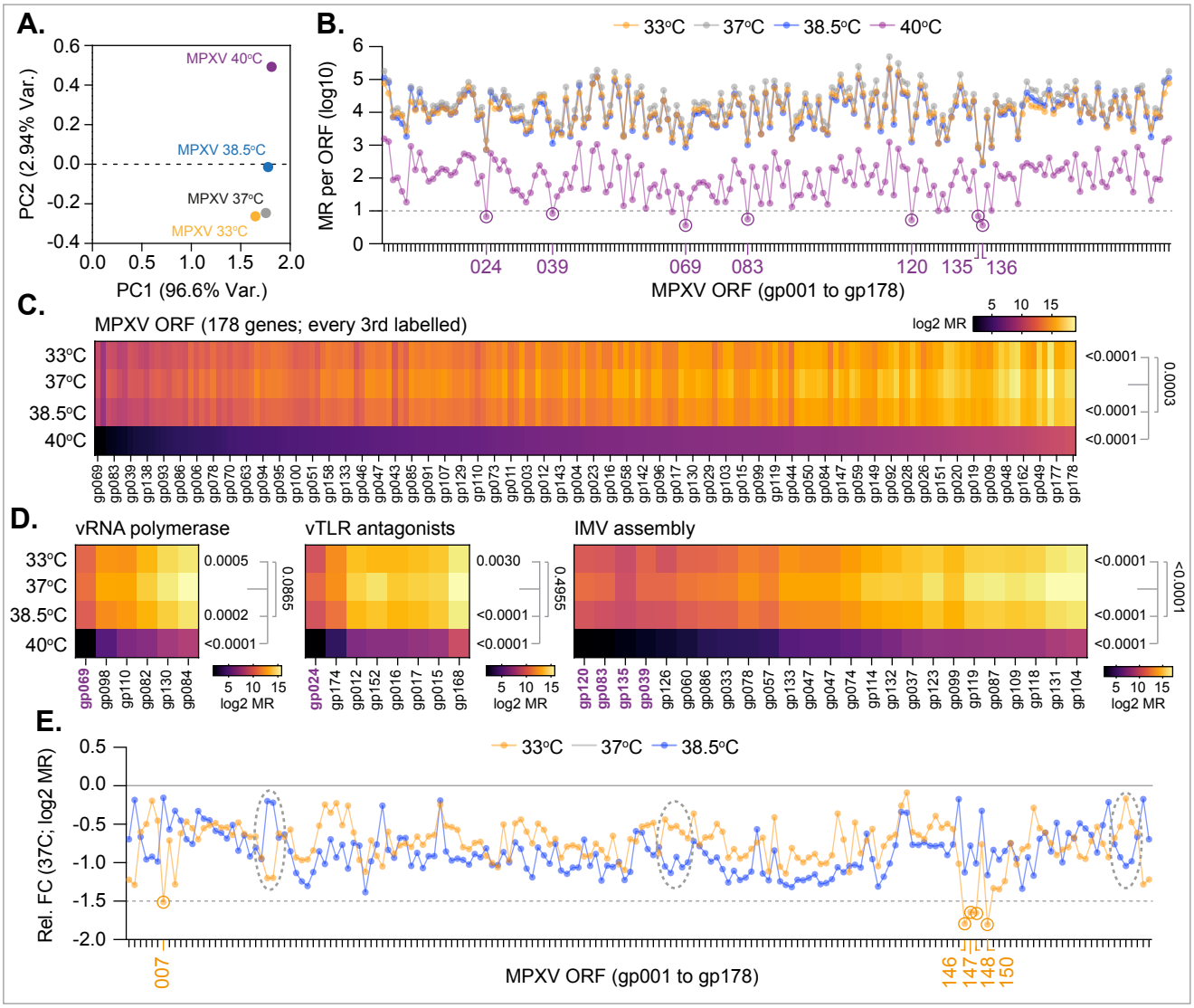

Figure 5. Basal host-cell temperature differentially influences the regulation of MPXV transcription

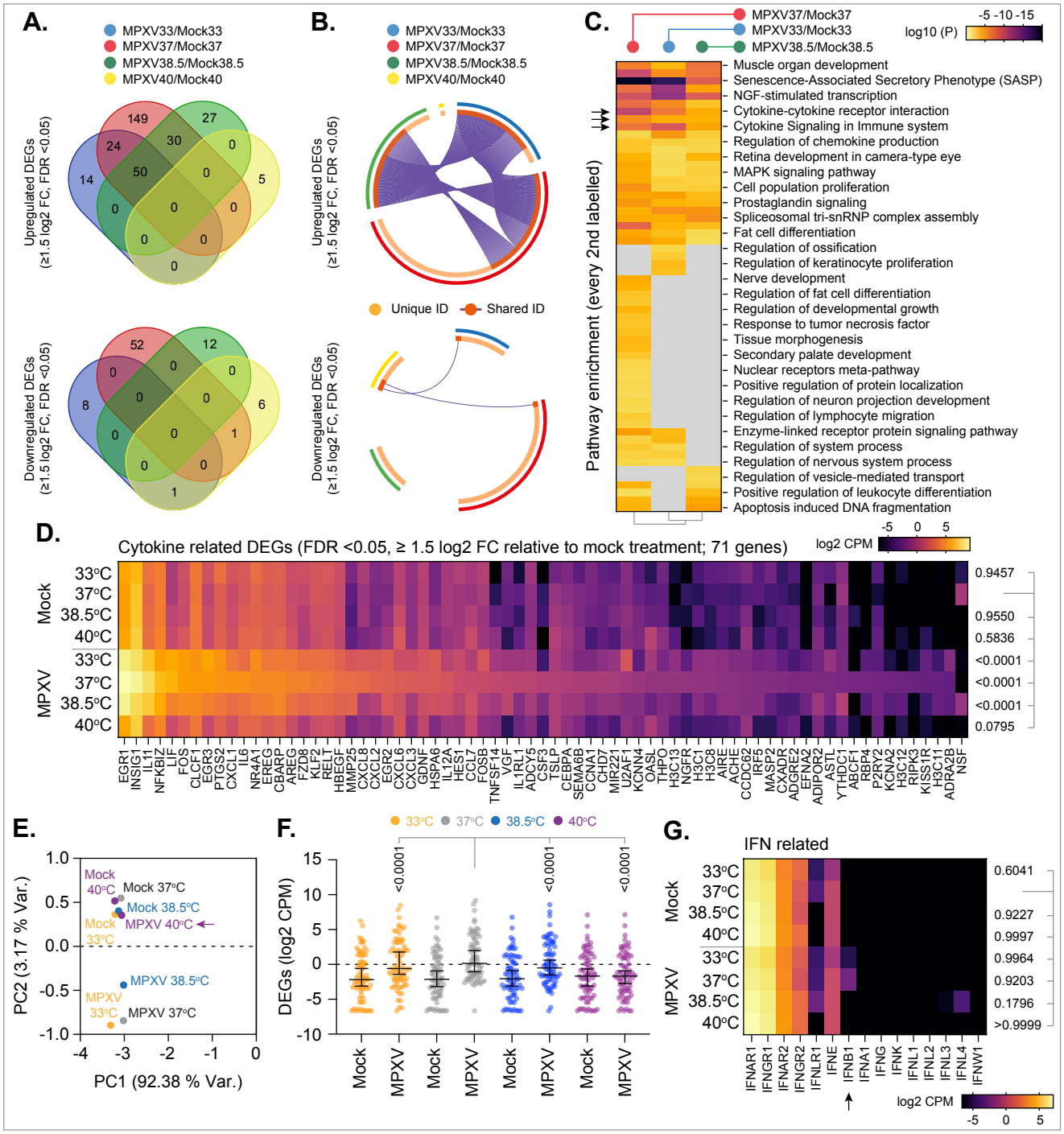

Figure 6: Basal temperature influences the host-cell response to MPXV infection

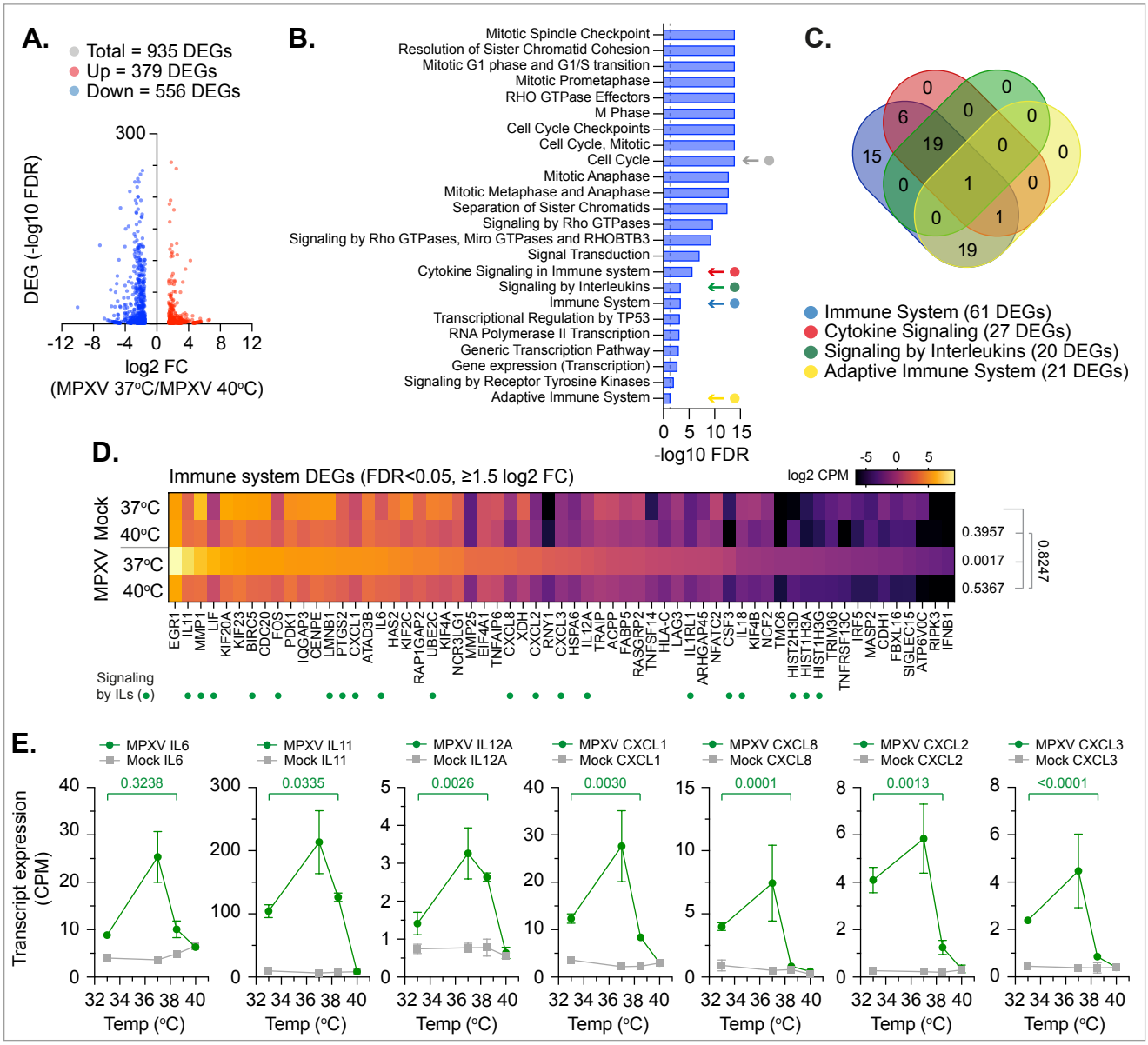

Figure 7: Basal host-cell temperature influences the interleukin response to MPXV infection

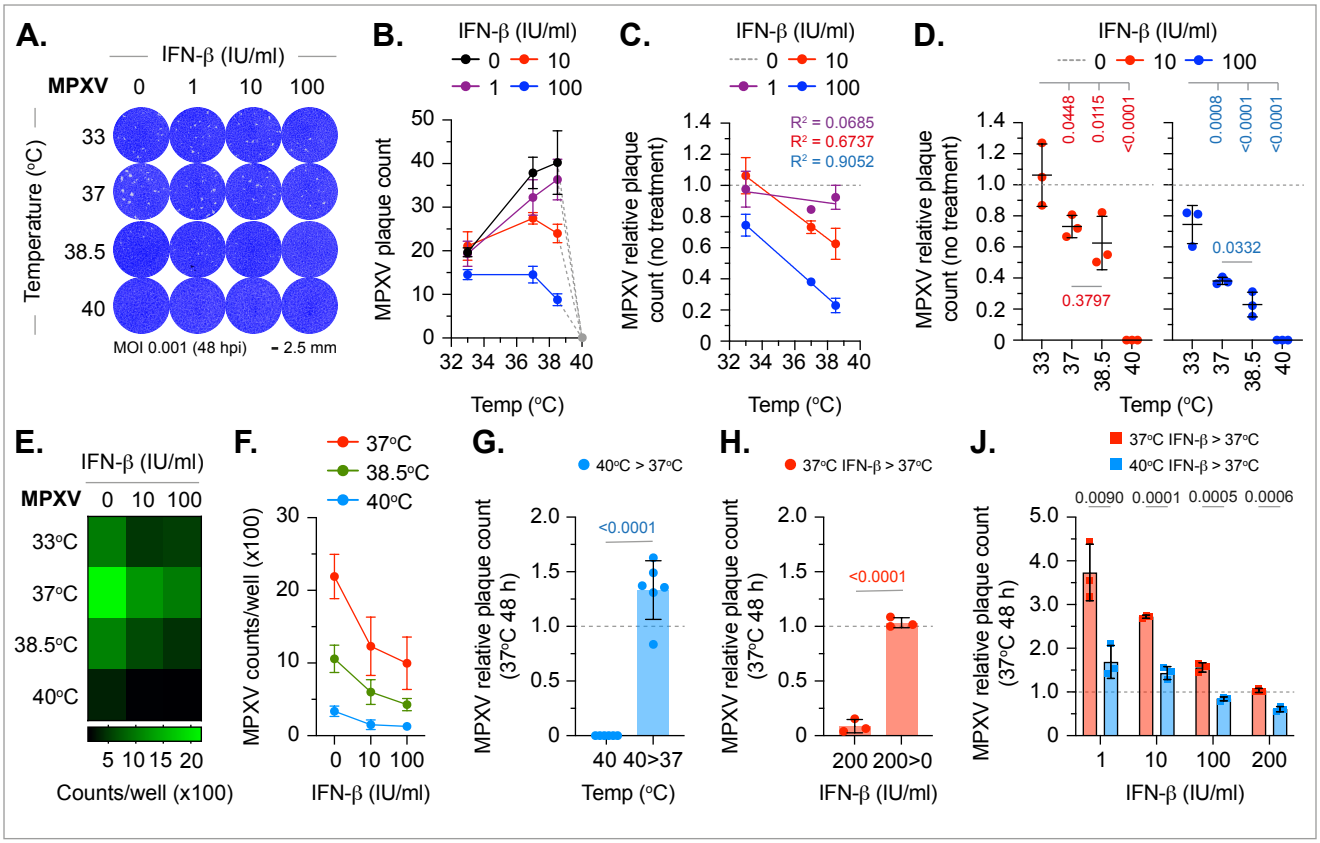

Figure 8: Temperature elevation enhances the type-I IFN-mediated host-cell restriction of MPXV

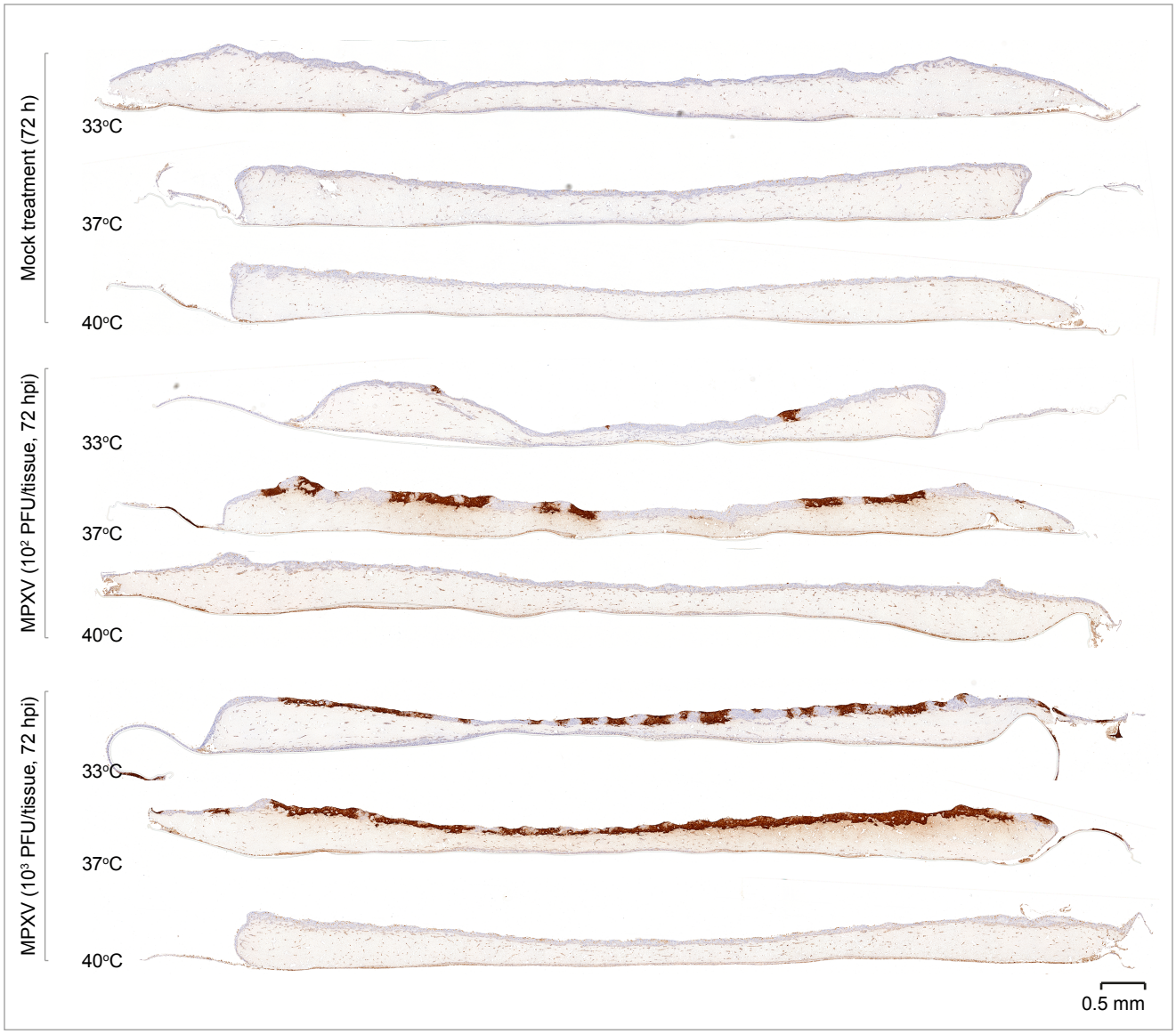

Figure S1. Tissue temperature influences the outcome of MPXV replication in skin epithelium

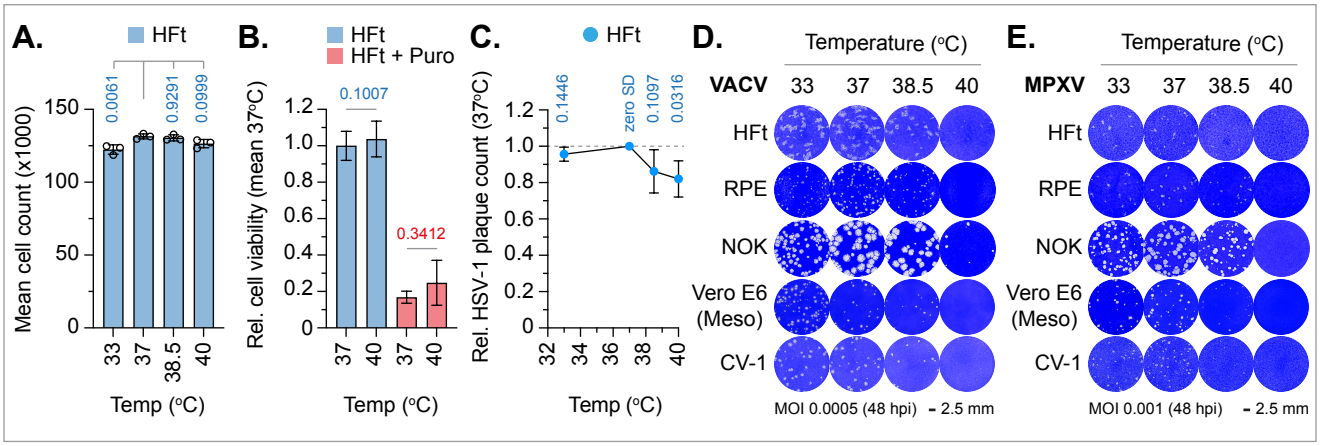

Figure S2. Temperature elevation inhibits orthopoxivurs replication.

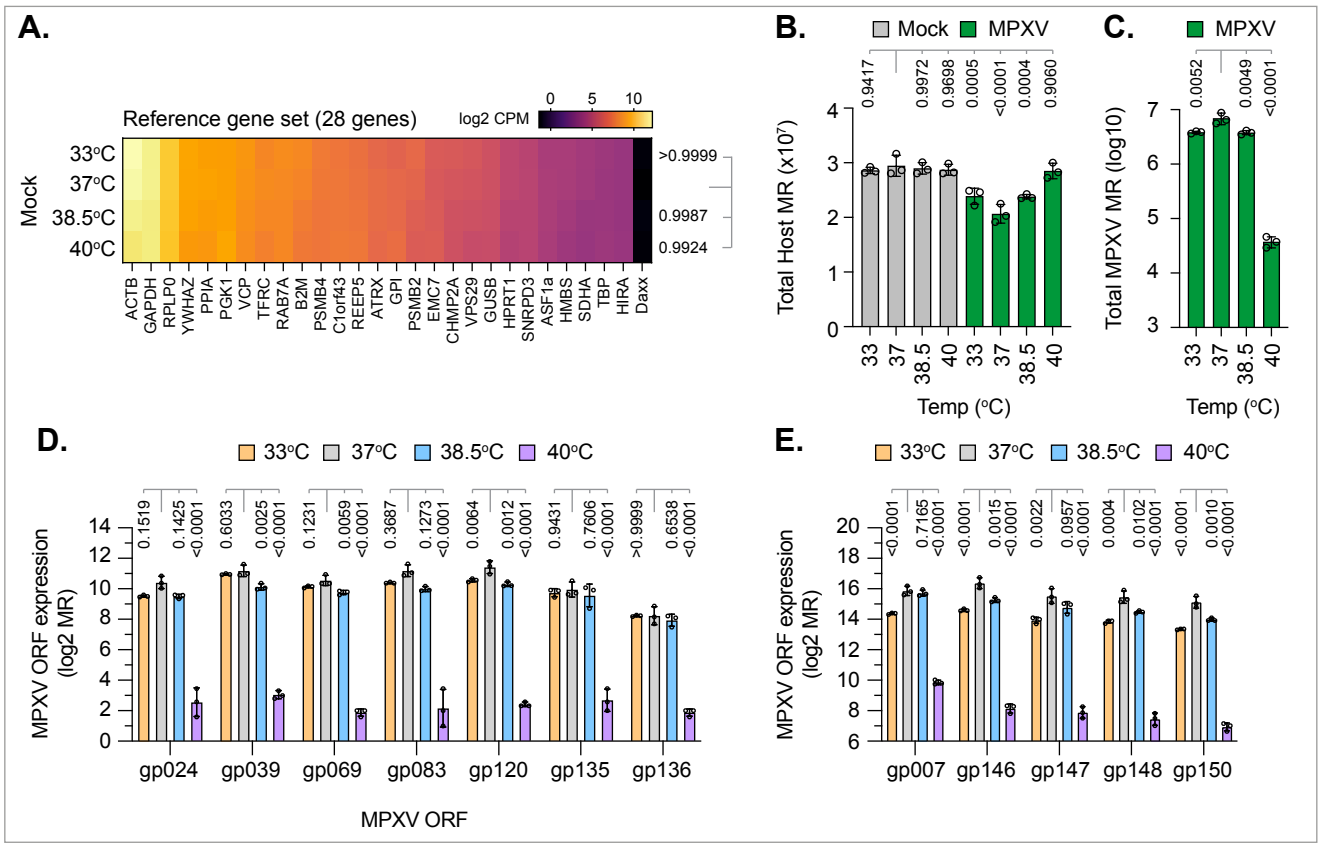

Figure S3: Basal host-cell temperature differentially influences MPXV transcription

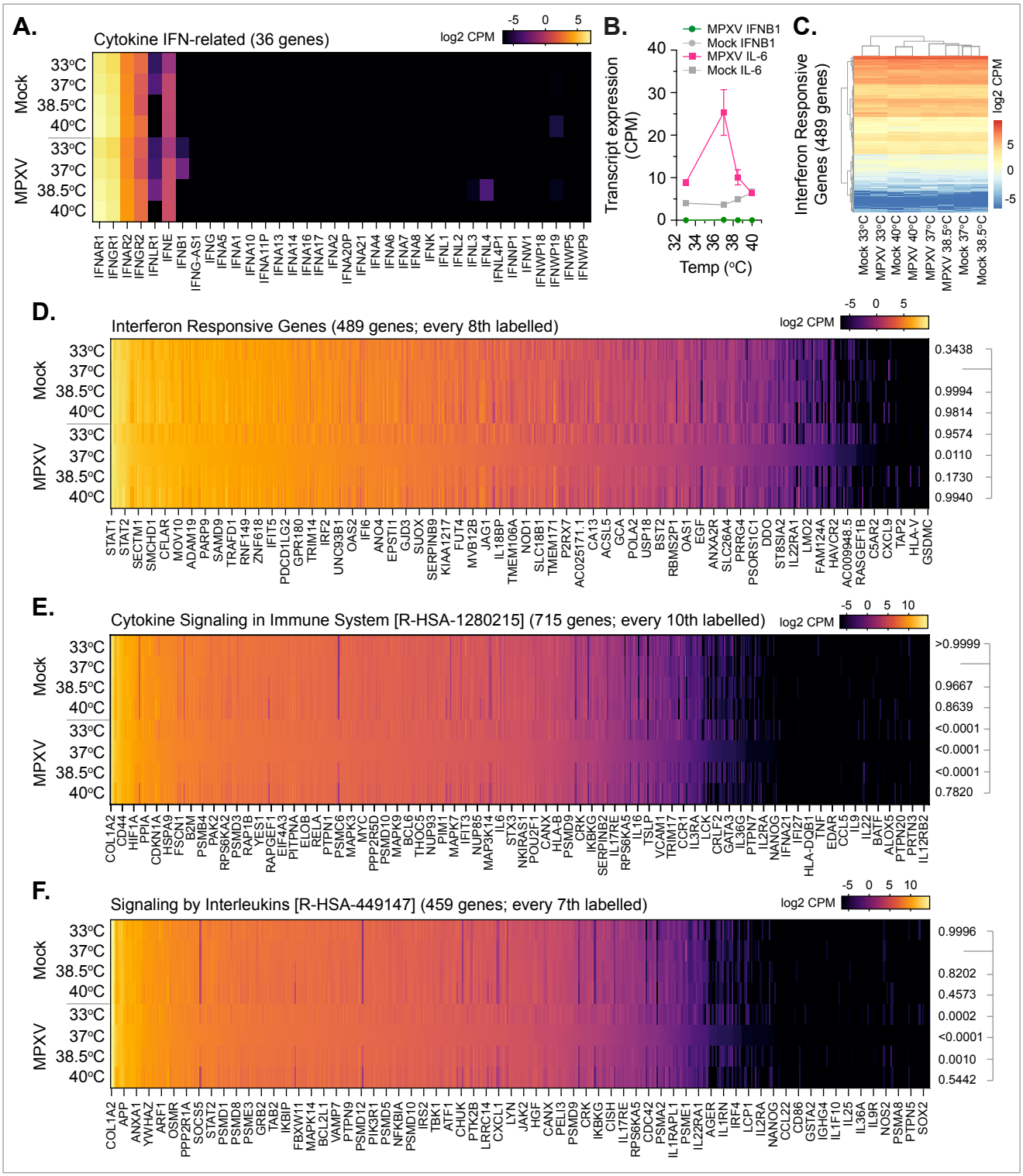

Figure S4. MPXV infection does not stimulate the induction of the type-I IFN respons

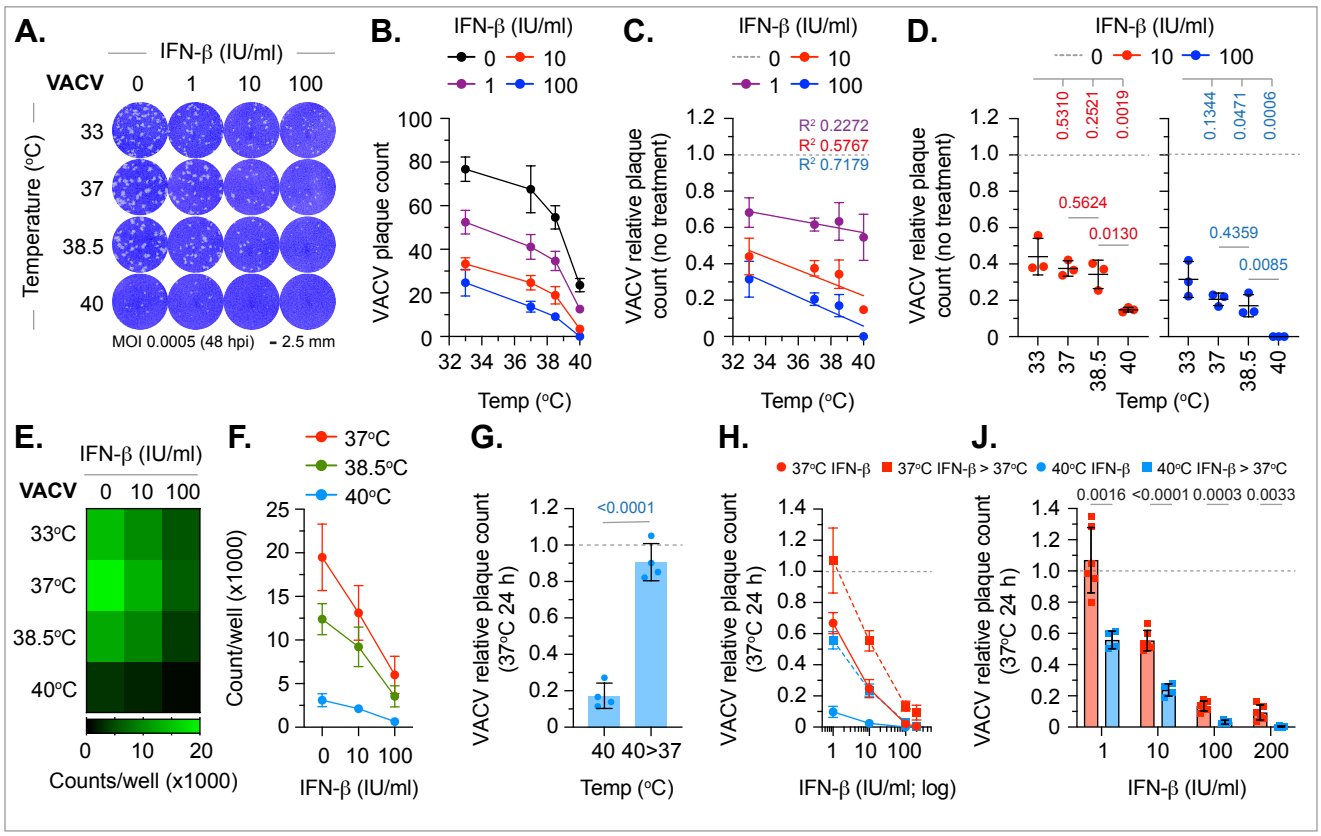

Figure S5. Temperature elevation enhances the type-I IFN-mediated host-cell restriction of VACV